NATIONAL UNIVERSITY OF SCIENCE AND TECHNOLOGY POLITEHNICA BUCHAREST

FACULTY OF CHEMICAL ENGINEERING AND BIOTECHNOLOGIES
DOCTORAL SCHOOL

DOCTORAL THESIS

Rapid Food Scanning Techniques for Enhancing National Security

PhD Student: Niculae Andreea-Roxana
Coordinator: Prof. Dr. habil Raluca-Ioana van Staden

2025

NATIONAL UNIVERSITY OF SCIENCE AND TECHNOLOGY POLITEHNICA BUCHAREST

FACULTY OF CHEMICAL ENGINEERING AND BIOTECHNOLOGIES DOCTORAL SCHOOL

DOCTORAL THESIS

Rapid Food Scanning Techniques for Enhancing National Security

PhD Student: Niculae Andreea-Roxana
Coordinator: Prof. Dr. habil Raluca-Ioana van Staden

Mentory Committee:

Name	Affiliation
Prof. Dr Eng. Gabriel Lucian Radu	Department of Analytical Chemistry and Environmental Engineering/National University of Science and Technology, Politehnica of Bucharest
Prof. Dr. Eugenia EftimieTotu	Department of Analytical Chemistry and Environmental Engineering/National University of Science and Technology, Politehnica of Bucharest
CSI Dr. Cătălina Neguț	Laboratory of Electrochemistry and PATLAB /National Institute for Research in Electrochemistry and Condensed Matter

Table of Contents

Contents

Introduction ……9

CHAPTER 1 - Food Security as a Dimension of National Security -The Role of Food Chemistry and Sensor-Based Detection 11

1.1. Food Security and National Security. Conceptual Framework 11

1.2. Romania's Agricultural Potential and Structural Challenges 12

1.3. Food Chemistry, Additives, and Contaminants 12

1.4. Implications for Food and National Security 15

CHAPTER 2 - Stochastic Sensors and Voltametric Sensor ……...16

2.1. Stochastic sensors ……...16

2.1.1. Mechanism of current development for stochastic sensors ……16

2.1.2. Design of the stochastic sensors ……17

2.1.3. Parameters of the stochastic sensors ……18

2.2. Voltametric sensors ……..…….....19

2.2.1. The construction of voltammetric sensors ……..19

2.2.2. The parameters of voltametric sensors ……...19

2.3. Voltametric sensors vs stochastic sensors in food analysis ……...21

CHAPTER 3 - Nanographene Based Electrochemical Sensors for Ultrasensitive Determination of Sorbic Acid from Food ……..……..24

3.1. Introduction ……24

3.2. Experimental ……..25

3.2.1. Materials and reagents ……25

3.2.2. Apparatus and methods ……..25

3.2.3. Design of the electrochemical sensor ……26

3.2.4. Samples preparation ……...26

3.3.Results and Discussions ……...……..26

3.3.1. SEM characterization of the active surface of the electrochemical sensors ……26

3.3.2. Electrochemical characterization of the sensors ……27

3.3.2.1.The influence of the pH value on the electrochemical behaviour of the sensors..30

3.3.3. Response characteristics of the electrochemical sensors ……...32

3.3.4. Interference studies ……..……..35

3.3.5. Reproducibility, repeatability and stability …….…..….36

3.4. Determination of sorbic acid in food ……...37

CHAPTER 4 - Enantioanalysis of limonene ……..……..39

4.1. Sulfur-doped graphene based electrochemical sensors for fast and sensitive determination of (R)-(+)-Limonene from beverages ……..……39

4.1.1. Introduction ……..……39

4.1.2 Materials and Methods ……...……40

4.1.3. Results and Discussion ……..……41

4.1.3.1. Electrochemical characterization of the sensor ……..……41

4.1.3.2. The influence of the pH value on the electrochemical behavior of the sensors ..45

4.1.3.3. Response characteristics of the electrochemical sensors ……..……46

4.1.3.4. Selectivity of the electrochemical sensor ……...50

4.1.3.5. Reproducibility, repeatability and stability ……..…….51

4.1.4. Determination of R-limonene in beverages ……..……..……54

4.2.Enantioanalysis of Limonene in Beverages Using Stochastic Sensors ……..…56

4.2.1. Introduction ……..…….56

4.2.2. Experimental ……..57

4.2.2.1. Materials and Methods ……..……..…57

4.2.2.2.Design of the enantioselective stochastic microsensors ……..58

4.2.2.3. Stochastic method of analysis ……..58

4.2.3. Results and Discussions ……..……..….58

4.2.3.1. Response characteristics of the stochastic microsensors ……..…58

4.2.3.2. Stability and reproducibility measurements ……..…60

4.2.3.3. Selectivity of the stochastic enantioselective microsensors ……..…60

4.2.4. Enantioanalysis of the limonene in beverages ……60

CHAPTER 5 - Determination of atrazine using voltametric and stochastic sensors…..64

5.1.Electroanalysis of atrazine in water and beverages using voltametric sensors …….64

5.1.1. Introduction ……..64

5.1.2. Experimental ……..……65

5.1.2.1. Materials and reagents ……..…65

5.1.2.2. Apparatus ……65

5.1.2.3. Design of the electrochemical sensor ……65

5.1.2.4. Recommended procedure ……..……65

5.1.2.5. Samples ……66

5.1.2.6. Selectivity studies ……..……..66

5.1.3. Results and discussions ……...….66

5.1.3.1.Characteristic response of the proposed electrochemical sensor …….……66

5.1.3.2.Selectivity of the electrochemical sensor ……68

5.1.4. Determination of atrazine in water and beverages samples…….…….68

5.2. Ultrasensitive assay of atrazine in food and water samples using stochastic sensors ……69

5.2.1. Introduction ……..……69

5.2.2. Materials and Methods ……..…….72

5.2.2.1. Materials ……..……..72

5.2.2.2. Methods ……..……...73

5.2.2.3.Design of stochastic platform ……...…73

5.2.2.4.Samples ……..78

5.2.3. Results and discussions ……79

5.2.3.1.Response characteristics of on-site screening platforms 79

5.2.3.2.The selectivity of the on-site screening platforms 81

5.2.4. Determination of atrazine in fruits, vegetables and water samples 81

CHAPTER 6 - Ultrasensitive and fast determination of ß-carotene in vegetables using stochastic sensors 84

6.1. Introduction 84

6.2. Experimental 85

6.2.1. Materials and Methods 85

6.2.2. Design of stochastic sensor 85

6.2.3. Samples 87

6.3. Results and discussions 87

6.3.1. Response parameters of the stochastic 3D sensor 87

6.3.2. The selectivity of the sensor when used to determine the ß-carotene ……88

6.4. Validation of the 3D stochastic sensor for the determination of ß-carotene in bell peppers, sweet potato and oranges ……..……88

CHAPTER 7 - Fast screening of biological and Food Samples Using Miniplatforms Based on 3D Stochastic Microsensors ……92

7.1.Introduction ……92

7.2.Experimental ……94

7.2.1.Materials and Methods ……94

7.2.2. Design of the Stochastic Sensor ……95

7.2.3. Method ……95

7.2.4. Samples ……96

7.3. Results and discussions ……96

7.3.1. Response characteristics of the miniplatforms based on 3D stochastic microsensors ……96

7.3.2. Selectivity ……98

7.4. Enantioanalysis of aspartic acid in food and biological samples ……99

CHAPTER 8 - Stochastic Determination of Ethyl Propionate in Commercial Juices..104

8.1. Introduction ……104

8.2. Materials and Methods ……106

8.2.1. Reagents and materials ……106

8.2.2. Apparatus ……106

8.2.3. The design of the 3D combined stochastic sensor ……106

8.2.4. Stochastic method ……107

8.2.5. Samples ……107

8.3. Results and discussions ……108

8.3.1. Response characteristics of the 3D combined stochastic sensor ……108

8.3.2. Selectivity of the 3D combined stochastic sensor ……109

8.4. Validation of the 3D combined stochastic sensor ……110

Conclusions ……113

Original contributions ……117

Future perspectives ……118

References ……119

Annex1 Participation in national and international conferences ……142

Annex 2 Paper published in ISI Journals ……144

Acknowledgements

First and foremost, I give thanks to God for His protection and guidance, and for leading me to the privilege of meeting Professor Raluca-Ioana van Staden, an extraordinary, dedicated person, without whom this achievement would not have been possible.

I would also like to express my deepest gratitude to my parents, Liliana and Iulian, for their unwavering moral and financial support, which has shaped me into who I am today.

My heartfelt thanks go as well to my colleagues, who have become true friends. Together we shared not only academic experiences, but also pieces of cake, laughter, tears, and countless moments that transformed us into a family.

A PhD journey is not only about learning and research, it is about personal growth, intellectual development, building lifelong friendships, and embracing valuable new experiences. All these together form a whole, one that I will always treasure.

Introduction

Food security became a very important issue especially because the quality of food may have a direct impact on the state of health of population [1]. Food security is connected not only with the additives, or by products resulting from the food degradation, or adulteration of food, but also to the nutrients that the people must take from food, because they are not produced by the body, their absence becoming a life-threatening issue [2-60].

Digitalisation of food control became a very important issue worldwide. On-site food control with transmission of the results in real time to state agency able to take a fast decision related to the food security is a high requirement seen in many papers published in different regions of the world [61-65].

Food adulteration is a big concern since old times, which contributes to the decrease of the quality of food [66,67]. Numerous techniques are available for detection of food adulteration [66]: molecular, physical, and biochemical (especially immunological) techniques were proposed to date. While most of the techniques used to detect the biological adulterants are molecular techniques, for the rest of the adulterants biochemical or physical techniques are preferred [66].

The concentration of proteins, and the types of proteins in food have an important role nowadays for the quality of food. While animal proteins may not be able to cover the needs until 2050 or 2100 (due to increase of population with few billions), alternative sources like plant-based proteins, single-cell proteins, cultured meat, insect protein are investigated [68]. Research performed to date shown that these alternative types of proteins have comparable nutritional benefits like the animal proteins [68].

The soil quality has an important role in food quality [69]. Crop diversification represents a sustainable strategy to reduce the risk of monoculture. The genetic, temporal, spatial, intercropping diversification improve the health of soil, pest management. This can also have an effect on reducing of utilisation of pesticides which may have an unhealthy effect on population.

Climate changes affect the agriculture, and soil quality. Global heating of earth, less rain, or acidic rains are usually influencing the quality of soil, of plants which may be reflected on the health of animals and population [70-72]. Integrating multiple climate-smart agriculture strategies may improve the health of the soil, as well as the food security [70, 71].

Most of the standard techniques used in food control are using either ELISA [73], chromatographic techniques (HPLC, GC coupled with MS) [74,75], or spectroscopic techniques [76], chemiluminescence techniques [77]. All of these techniques of analysis have the following disadvantages: are expensive, the sample must be processed before its analysis, high amounts of samples are needed for analysis, it is impossible to perfume an on-site determination of quality of food.

Therefore, the main objective of this PhD thesis was to find fast reliable techniques for screening of food for increasing the food security. Specific objectives of the thesis were: the design of new tools for screening of food; characterisation and validation of the tools used for the screening of food; publication of minimum 5 articles in ISI journals.

To achieve the objectives, electrochemical sensors and stochastic sensors were selected as new tools for screening of food. These are the only tools that can be used for on-site analysis of food. A reliable qualitative analysis can be performed using the stochastic sensors. Screening of food samples and beverages were performed with high reliability for the enantioanalysis of limonene and aspartic acid, as well as for the determination of sorbic acid, atrazine, ß-carotene, and ethyl propionate. The proposed tools and screening techniques proved to be valuable alternative of the standard method used for the quality control of food, and food security, having the main advantage their ability of performing high reliable qualitative and quantitative analysis, and the ability of screening on-site the food samples, providing results in real time, that can be fitted into specialised data bases available for population protection authorities which can take act if foods contain substances that can be a threaten to the health of the population.

CHAPTER 1

Food Security as a Dimension of National Security

The Role of Food Chemistry and Sensor-Based Detection

Food security is a multidimensional concept directly linked to national security, encompassing not only agricultural production and food availability but also food safety, nutritional quality, and consumer trust [2-61]. Romania, with its vast agricultural potential, faces persistent vulnerabilities that can undermine its resilience in times of crisis. In this regard, food chemistry research and the application of rapid, sensor-based detection methods for toxic substances represent a critical step forward in strengthening food security at both national and European levels.

CHAPTER 2

Stochastic Sensors and Voltametric Sensor

2.1. Stochastic sensors

Stochastic sensors represent a new class of electrochemical sensors with special characteristics making them valuable tools for determination of small quantities of substances from very complex matrices. Proposed by Bayley and Cremer in 2001 [78], as sensors inspired by biology. Four years later, Schmidt shown further the mechanism of stochastic signal development [79]. This type of sensors was used to date for many types of analysis including biomedical analysis, environmental analysis, and food analysis of organic and inorganic type of molecules [80-89].

2.1. Voltametric sensors

Voltametric sensors are intensively used for food analysis. Very good selectivity is usually recorded by using this type of sensors [92, 93]. The differential pulse voltammetry is

the most used technique involving this type of sensors as tools. High sensitivities are usually recorded when this technique is employed.

ORIGINAL CONTRIBUTIONS

CHAPTER 3

Nanographene Based Electrochemical Sensors for Ultrasensitive Determination of Sorbic Acid from Food [96]

3.3.1. Response characteristics of the electrochemical sensors

The response characteristics of the proposed electrochemical sensors were determined using square-wave voltammetry, at the optimum pH value (2.0), and are summarized in Table 3.1.

Table 3.1. Response characteristics of the electrochemical sensors used for the determination of sorbic acid.

Parameter	Electrochemical sensor	
	ZnPIX/AuNPs-Gr sensor	Mn(TPP)Cl/AuNPs-Gr sensor
Equation of calibration*	Ip_a=-5.29+0.22xC; r=0.9985	Ip_a=-5.01+0.35xC; r=0.9984
Linear concentration range (µmol L^{-1})	1.0-1x10^3	1.0-1x10^3
Sensitivity (nA/µmol L^{-1})	0.22±0.03	0.35±0.02
Limit of detection (µmol L^{-1})	0.33	0.33
Limit of determination (µmol L^{-1})	1.00	1.00
Repeatability of peak current (%, RSD)	5.56	5.41

*<Ip_a>=nA; <C>=µmol L^{-1}

Optimized working conditions coupled with the electrocatalytic capacity of the porphyrins selected for the sensors' design, favorized the obtaining of high sensitivities and low limits of quantification and determination for the proposed sensors.

Figure 3.7 showed for the ZnPIX/AuNPs-Gr sensor the peaks obtained during the calibration as well as the calibration graph for sorbic acid. The linear concentration range was between 1.00 and 1000 µmol L^{-1} with a correlation coefficient of 0.9985. The limit of detection was

0.33 µmol/L, which was calculated as a third from the limit of quantification (the lowest concentration from the linear concentration range, 1 µmol L^{-1}). The sensitivity of the ZnPIX/AuNPs-Gr sensor was 0.22 nA μmol^{-1} L.

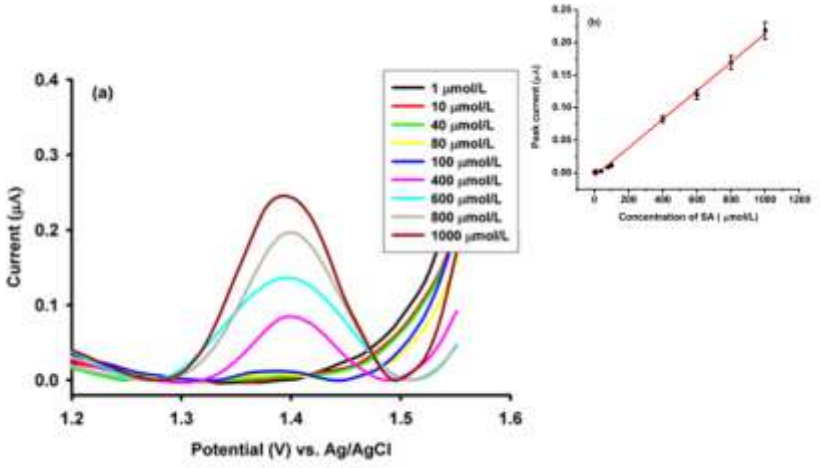


Figure 3.7. (a) Square-wave voltammograms recorded with the ZnPIX/AuNPs-Gr sensor in PBS pH = 2.0 containing different concentrations of sorbic acid (1 to 1000 µmol L^{-1}); (b) Calibration graph obtained with the ZnPIX/AuNPs-Gr sensor from 1 to 1000 µmol L^{-1}. Working conditions: step potential of 0.025 V and frequency of 5.0 Hz.

Figure 3.8. showed the voltammograms obtained during the calibration of the Mn(TPP)Cl/AuNPs-Gr sensor, as well as the calibration graph for sorbic acid. The linear concentration range was between 1.00 and 1000 µmol L^{-1}. The limit of detection (calculated as a third from the limit of quantification) was 0.33 µmol L^{-1}. The sensitivity recorded for this sensor was 0.35 nA μmol^{-1} L.

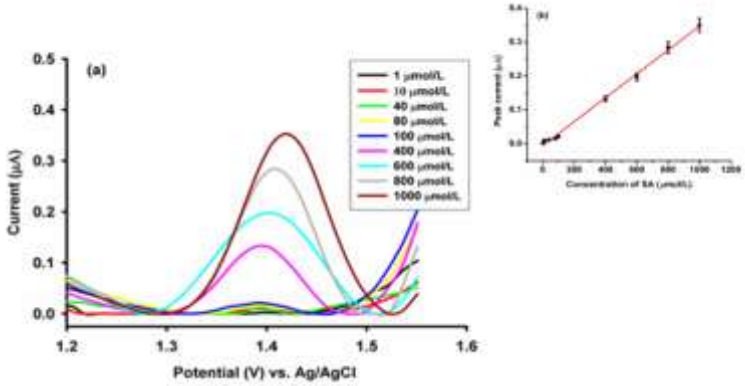
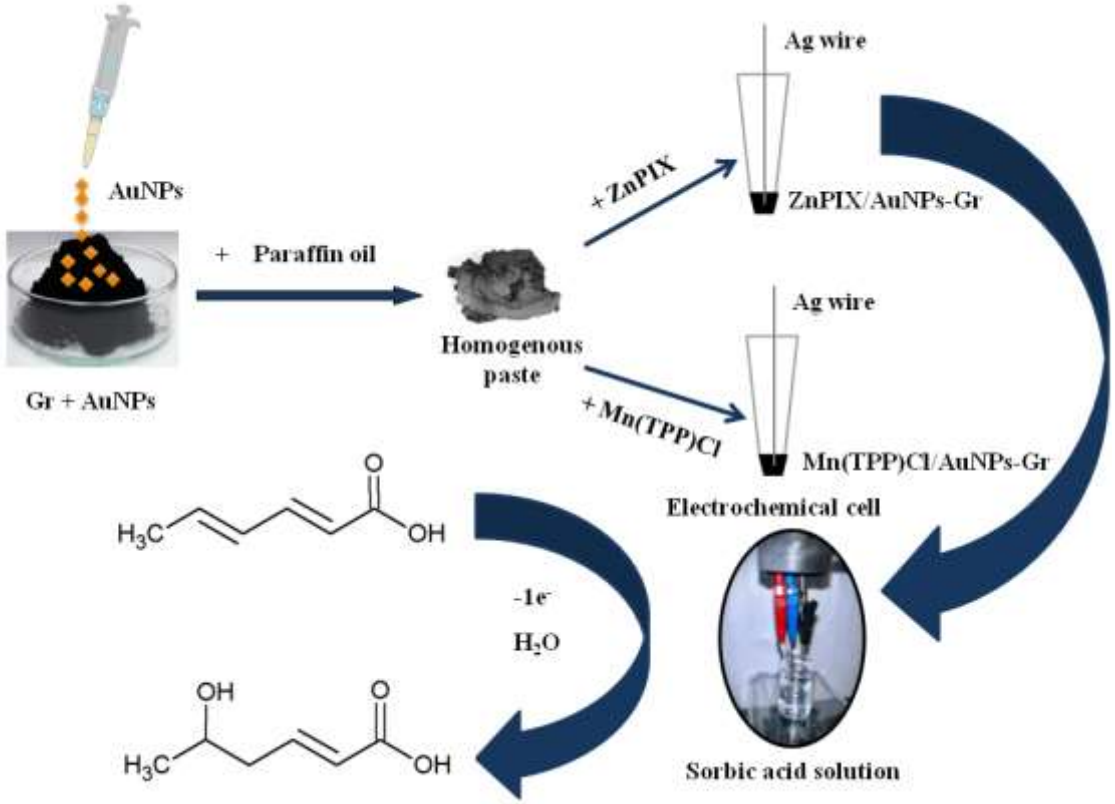


Figure 3.8. (a) Square-wave voltammograms recorded with the Mn(TPP)Cl/AuNPs-Gr sensor in PBS pH = 2.0 containing different concentrations of sorbic acid (1 to 1000 µmol L^{-1}); (b) Calibration curve obtained with the Mn(TPP)Cl/AuNPs-Gr sensor from 1 to 1000 µmol L^{-1}. Working conditions: step potential of 0.025 V and frequency of 5.0 Hz.



Scheme 3.1. Schematic representation of the electrodes design and the possible mechanism of the electrochemical oxidation of sorbic acid in acidic media (pH = 2.0)

The possible mechanism of reaction of sorbic acid is presented in Scheme 3.1., and involves the breaking of one double bond and the addition of OH^- followed by the chemical deprotonation of the oxidation product.

While the limits of quantification and detection as well as the linear concentration ranges are the same for both sensors, the sensitivity of the Mn(TPP)Cl/AuNPs-Gr sensor is higher compared with the sensitivity recorded for the ZnPIX/AuNPs-Gr sensor. Therefore, this is the sensor of choice. Comparing with the methods proposed earlier [96-104], the proposed sensors are more sensitive, the limits of quantification and determination are lower, and the linear concentration range is wider.

Table 3.4. Determination of sorbic acid in white bread, brown bread and mayonnaise samples using the ZnPIX/AuNPs-Gr sensor.

Sample	Amount added (µmol L^{-1})	Amount found (µmol L^{-1})	Recovery (%)	RSD %*
White bread sample	400	386.41	96.60	0.71
	800	787.72	98.47	1.25
Brown bread sample	400	393.12	98.28	3.93
	800	791.00	98.88	1.63
Mayonnaise	400	384.68	96.17	0.76
	800	798.21	99.78	3.62

*N=10

Table 3.5. Determination of sorbic acid in white bread, brown bread and mayonnaise samples using the Mn(TPP)Cl/AuNPs-Gr sensor.

Sample	Amount added (µmol L^{-1})	Amount found (µmol L^{-1})	Recovery (%)	RSD %*
White bread sample	400	389.85	97.46	4.58
	800	773.53	96.69	0.24
Brown bread sample	400	381.01	95.25	2.98
	800	791.56	98.94	2.84
Mayonnaise	400	397.19	99.30	0.81
	800	761.40	95.17	0.33

*N=10

The results shown in Tables 3.4. and 3.5. shown high reliability of the assay of sorbic acid in white and brown bread as well as in the mayonnaise. When the ZnPIX/AuNPs-Gr sensor was used, the recoveries were higher than 96.00% for white bread with RSD, less than 1.50%; higher than 98.00% for brown bread with RSD values less than 4.00%; while for the mayonnaise, the recovery was higher than 96.00% with RSD values less than 4.00% (Table 3.4.). When the Mn(TPP)Cl/AuNPs-Gr sensor was used, the recoveries were higher than 96.50% for white bread with RSD, less than 5.00%; higher than 95.00% for brown bread with RSD values less than 3.00%; while for the mayonnaise, the recovery was higher than 95.00%

with RSD values less than 1.00% (Table 3.5). Accordingly, the proposed sensors can be used for the assay of sorbic acid in white/brown bread and mayonnaise.

The choice of sensors based on modification of nanographene paste decorated with gold nanoparticles with metal porphyrins (Zn protoporphyrin IX, and 2,3,7,8,12,13,17,18 octaethyl, 21H, 23H-porphirine Mn(III) chloride) proved to increase the sensitivity and the selectivity of the assay of sorbic acid in food; also, the recoveries recorded were very high with low RSD (%) values.

CHAPTER 4

Enantioanalysis of limonene

4.1. Sulfur-doped graphene based electrochemical sensors for fast and sensitive determination of (R)-(+)-Limonene from beverages [113]

4.1.3. Results and Discussion

4.1.3.3. Response characteristics of the electrochemical sensors

The response characteristics of the modified electrochemical sensors were determined by differential pulse voltammetry, at the optimum pH of 2.0 for the TPP/AuNPs-S-Gr sensor and pH of 3.0 for the Fe(TPFPP)Cl/AuNPs-S-Gr sensor. The results obtained are presented in Table 4.1.

Figure 4.6. (a) showed for the TPP/AuNPs-S-Gr sensor the peaks obtained during calibration, as well as the calibration graph for R-LIM. The linear concentration range was between 1×10^{-5} and 6×10^{-4} mol L^{-1} with a good regression coefficient.

The limit of detection (LOD) was 3×10^{-6} mol L^{-1} and the limit of quantification (LOQ) was 1×10^{-5}. LOD and LOQ were calculated as follows: LOD = 3s/m, LOQ = 10s/m; where s – standard deviation of the peak current of the blank (4 measurements) and m – the slope of the calibration curve. The sensitivity of the TPP/AuNPs-S-Gr sensor was 0.7068 μA/mol L^{-1}.

Table 4.1. Response characteristics of the electrochemical sensors used for the detection of R-limonene.

Parameter	Electrochemical sensors	
	TPP/AuNPs-S-Gr	**Fe(TPFPP)Cl/AuNPs-S-Gr**
Equation of calibration*	$Ip_a = 0.0014(\pm0.0003) + 0.7068 \times C$; $R^2 = 0.9966$	$Ip_a = 0.0002(\pm0.0001) + 0.5027 \times C$; $R^2 = 0.9983$
Linear concentration range (mol L^{-1})	$1 \times 10^{-5} – 6 \times 10^{-4}$	$1 \times 10^{-5} – 1 \times 10^{-3}$
Sensitivity (µA/mol L^{-1})	0.7068±0.0020	0.5027±0.0014
Limit of detection (mol L^{-1})	3×10^{-6}	3×10^{-6}
Limit of quantification (mol L^{-1})	1×10^{-5}	1×10^{-5}
Repeatability of peak current (%, RSD)	2.48	3.24

* <Ip_a>=µA; <C>=mol L^{-1}, N=10

The dependence between the peak current and the concentration of R-LIM was linear (Fig. 4.

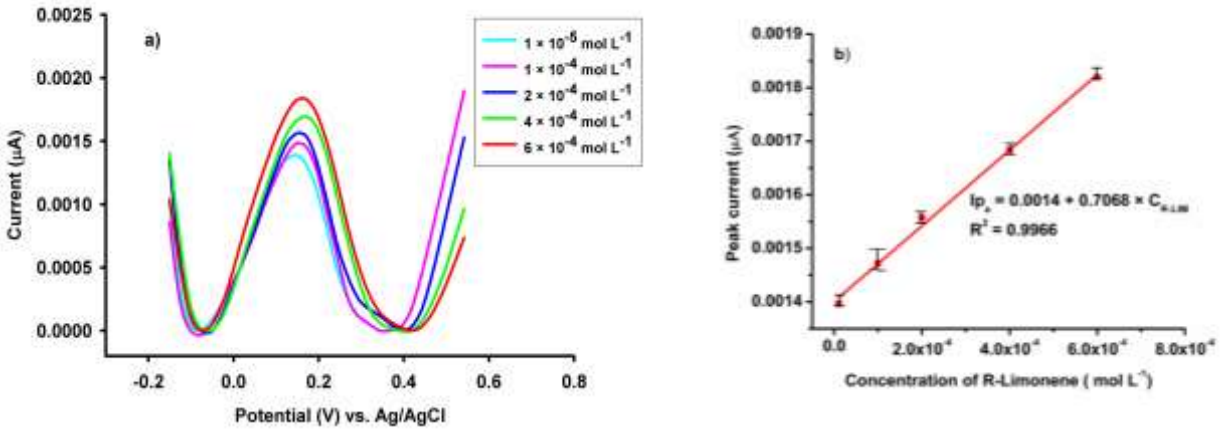


Figure 4.6. (a) Differential pulse voltammograms recorded with the TPP/AuNPs-S-Gr sensor in PBS pH 2.0 containing different concentrations of R-limonene from 1×10^{-5} mol L^{-1} to 6×10^{-4} mol L^{-1}; (b) Calibration curves obtained with the TPP/AuNPs-S-Gr sensor from 1×10^{-5} mol L^{-1} to 6×10^{-4} mol L^{-1}. Working conditions: step potential of 0.025 V; scan rate of 0.025 V s^{-1}.

For the Fe(TPFPP)Cl/AuNPs-S-Gr sensor, Figure 4.7. (a) showed the peaks obtained during calibration, as well as the calibration graph for R-LIM. The linear concentration range was between 1×10^{-5} and 1×10^{-3} mol L^{-1}. The LOD and LOQ were calculated to be 3×10^{-6} mol L^{-1} and 1×10^{-5} mol L^{-1}, respectively. These were calculated using the above formulas. The sensitivity of the Fe(TPFPP)Cl/AuNPs-S-Gr sensor was 0.5027 µA/mol L^{-1}.

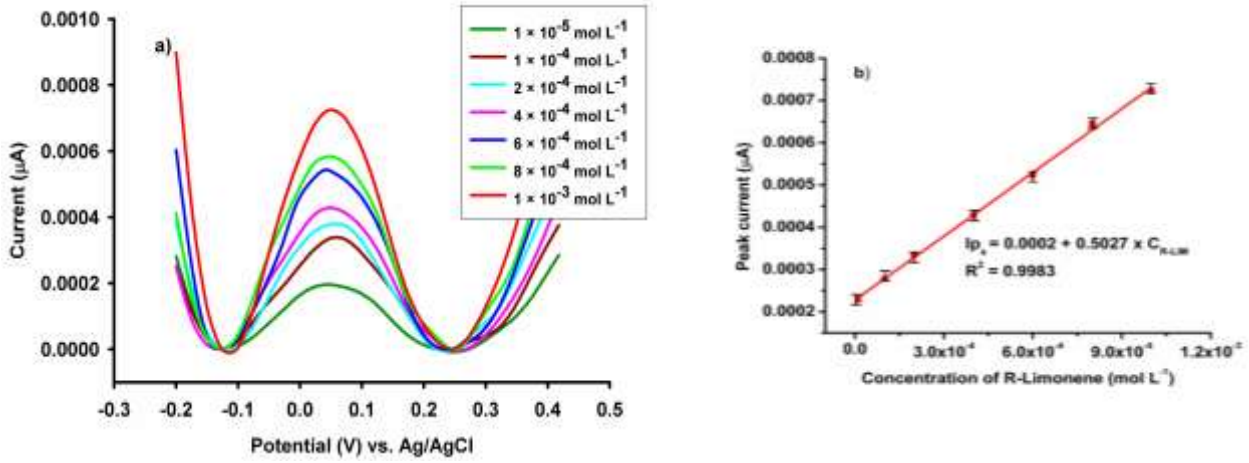


Figure 4.7. (a) Differential pulse voltammograms recorded with the Fe(TPFPP)Cl/AuNPs-S-Gr sensor in PBS pH 3.0 containing different concentrations of R-limonene from 1×10^{-5} mol L^{-1} to 1×10^{-3} mol L^{-1}; (b) Calibration curves obtained with the Fe(TPFPP)Cl/AuNPs-S-Gr sensor from 1×10^{-5} mol L^{-1} to 1×10^{-3} mol L^{-1}. Working conditions: step potential of 0.025 V; scan rate of 0.025 V s^{-1}.

Table 4.4. Comparison between performances of chromatographic methods and the proposed electrochemical method.

Method	Linear concentration range	Limit of detection	Reference
HPLC/MS	0.10-0.75 pg mL^{-1}	0.06 pg mL^{-1}	[8]
GC/MS	3.00-20.00 ng mL^{-1}	1.70 ng mL^{-1}	[28]
Electroanalysis using Fe(TPFPP)Cl/AuNPs-S-Gr sensor	1.94 µg mL^{-1} – 1.94 mg mL^{-1}	580 ng mL^{-1}	This work
Electroanalysis using TPP/AuNPs-S-Gr sensor	1.94 µg mL^{-1} – 1.17 mg mL^{-1}	580 ng mL^{-1}	This work

As is can be seen, the proposed method is working for higher concentrations of limonene, and wider linear concentration ranges were obtained. The advantage of the proposed sensors versus chromatographic techniques are: no dilution of the beverage sample will be needed, because the concentration of R(+)-limonene is within the linear concentration ranges; the method proposed is cost-effective, and minimum pre-treatment (buffering) of samples is needed.

4.1.4. Determination of R-limonene in beverages

It is very important to validate the proposed sensors because their effectiveness is essential for their subsequent use in food quality control and food safety at the same time. We used the standard addition method for both sensors to validate them and to demonstrate that they are very reliable for R-LIM analysis in alcoholic beverages, such as limoncello and triple sec liqueur. We prepared the samples as shown above and for each of the samples, the R-LIM concentration was determined. After this step, known amounts of R-LIM were added, followed by measurements of its concentration. The results presented in the Table 4.5. showed high reliability of the R-LIM test in limoncello and triple sec liqueur. When we used the TPP/AuNPs-S-Gr sensor, the recoveries were approximately 99.00% for both samples with RSD values between 0.42 - 2.47%. When we used the Fe(TPFPP)Cl/AuNPs-S-Gr sensor, the recoveries were greater than 99.00% for both samples, with a maximum RSD value of 2.90% for the Limoncello sample and a maximum RSD value of 4.12% in the case of the triple sec liqueur sample (Table 4.6.). Consequently, the proposed sensors can be used for R-LIM analysis in limoncello and triple sec liqueur. Sensors based on sulfur-doped graphene paste and gold nanoparticles modified with 5,10,15,20-tetraphenyl 21H,23H-porphine and 5,10,15,20-tetrakis (pentafluorophenyl) -21H,23H porphyrin iron (III) chlorides, have shown an increase the selectivity for the detection of R-LIM in alcoholic beverages; also, the recorded recoveries were high and with low RSD values (%).

Table 4.5. The effect of coexisting species on the detection of 1×10^{-4} R-limonene (n = 5) using the TPP/AuNPs-S-Gr sensor.

Samples	Amount added (mol L^{-1})	Amount found (mol L^{-1})	Recovery (%)	RSD %
	-	2.83×10^{-5}	-	1.21
Limoncello	1×10^{-5}	9.92×10^{-6}	99.20	2.33
	1×10^{-4}	9.92×10^{-5}	99.23	1.34

	2×10^{-4}	1.98×10^{-4}	99.14	1.87
Triple sec liqueur	-	1.41×10^{-5}	-	2.47
	1×10^{-5}	9.90×10^{-6}	99.01	0.42
	1×10^{-4}	9.91×10^{-5}	99.15	0.71
	2×10^{-4}	1.99×10^{-4}	99.34	1.61

Table 4.6. Detection of R-Limonene in limoncello and liqueur triple sec samples using the Fe(TPFPP)Cl/AuNPs-S-Gr sensor.

Samples	**Amount added (mol L^{-1})**	**Amount found (mol L^{-1})**	**Recovery (%)**	**RSD %**
Limoncello	-	1.71×10^{-5}	-	1.95
	1×10^{-5}	9.92×10^{-6}	99.20	0.56
	1×10^{-4}	9.94×10^{-5}	99.38	2.90
	2×10^{-4}	2.00×10^{-4}	99.78	3.08
Triple sec liqueur	-	4.24×10^{-5}	-	0.77
	1×10^{-5}	9.99×10^{-6}	99.90	2.25
	1×10^{-4}	9.93×10^{-5}	99.31	4.12
	2×10^{-4}	2.00×10^{-4}	99.84	0.51

Recoveries of R-limonen in the presence of S-limonen were performed to prove the enantioselectivity of the proposed sensors; results are shown in Table 4.6.

Table 4.7. Recovery of R-limonene in the presence of S-limonene (N=10).

Sensor	**S-limonene, % Recovery**			
	R:S, mol:mol			
	2:1	**1:1**	**1:2**	**1:100**
TPP/AuNPs-S-Gr	99.31±0.05	99.87±0.03	99.30±0.02	99.43±0.03
Fe(TPFPP)Cl/AuNPs-S-Gr	99.48±0.07	99.21±0.05	99.50±0.06	99.47±0.05

Results shown in Table 4.7. shown that R-limonene can be determined in the presence of S-limonene despite the ratio between the two enantiomers.

4.2. Enantioanalysis of Limonene in Beverages Using Stochastic Sensors [142]

4.2.2. Results and Discussions

4.2.2.1.Response characteristics of the stochastic microsensors

Stochastic sensing relies on the conductivity of a channel, with two phases: the first, in which the analyte passes through the channel and blocks it (the time at which the channel is blocked is known as the signature of the enantiomer, and marked on the diagram as t_{off}, and its value provides information about the enantiomers), and the second, in which the analyte binds to the channel wall and promotes electrochemical processes (known as quantitative phase and marked in the diagram as t_{on}).

The processes taking place in the channel are:

Ch(i) + S-limonene(i) ⇔ Ch - S-limonene(i) (1)

Ch(i) + R-limonene(i) ⇔ Ch - R-limonene(i) (2)

where Ch is the channel, and i is the membrane-solution interface. The response characteristics are shown in Table 4.8.

Table 4.8. Response characteristics of the stochastic enantioselective microsensors.

Stochastic microsensor based on	Signature, t_{off} (s)	Equation of calibration*, R	Working conc. range (mol L^{-1})	Sensitivity, (s^{-1} mol^{-1} L)	Limit of determination (mol L^{-1})
		S-limonene			
TPP/Gr	1.9	$1/t_{on}=0.43+6.81\times10^{10}C$ r=0.9999	1×10^{-13}-1×10^{-4}	6.81×10^{10}	1×10^{-13}
[Fe(TPFPP)]Cl/ Gr	1.4	$1/t_{on}=0.64+1.36\times10^{13}C$ r=0.9998	1×10^{-15}-1×10^{-4}	1.36×10^{13}	1×10^{-15}
		R-limonene			
TPP/Gr	1.7	$1/t_{on}=0.32+2.17\times10^{12}C$ r=0.9989	1×10^{-14}-1×10^{-5}	2.17×10^{12}	1×10^{-14}
[Fe(TPFPP)]Cl/ Gr	1.0	$1/t_{on}=0.24+4.75\times10^{10}C$ r=0.9992	1×10^{-13}-1×10^{-5}	4.75×10^{10}	1×10^{-13}

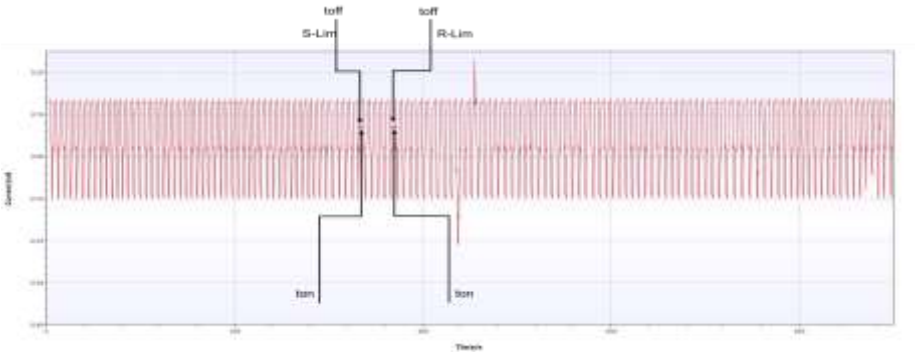
* <C> = mol L^{-1} $<t_{on}>$=s.

The signatures of S- and R-limonene are different for each of the stochastic microsensor proving that they can be determined simultaneously from beverages, and that the stochastic microsensors are enantioselective. The working concentration ranges are wide, making possible their assay from few fmol L^{-1} until few μmol L^{-1}. The highest sensitivity for the assay of S-limonene was recorded when the stochastic enantioselective microsensor based on Fe(TPFPP)]Cl/Gr was used, while for the assay of R-limonene, the highest sensitivity was

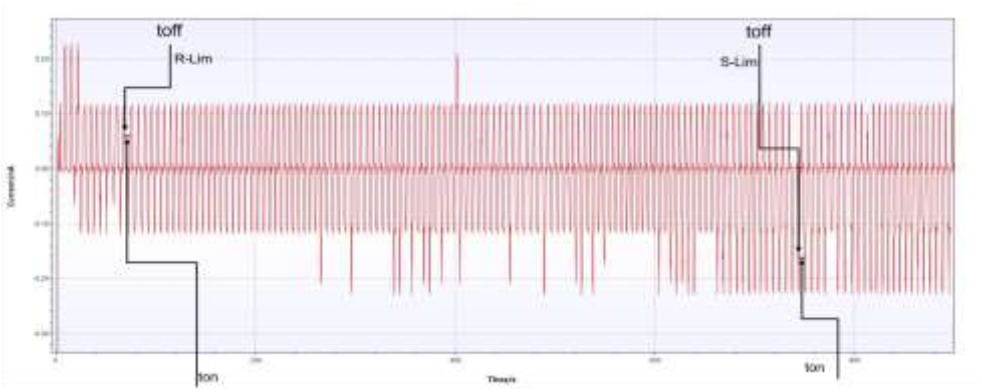
recorded when the stochastic enantioselective microsensor based on TPP/Gr was used. The lowest limit of determination was recorded for the assay of S-limonene when the stochastic enantioselective microsensor based on Fe(TPFPP)]Cl/Gr was used, while for the assay of R-limonene, the lower limit of determination was recorded when the stochastic enantioselective microsensor based on TPP/Gr was used. The advantage of utilization of these stochastic enantioselective microsensors versus the voltametric ones reported earlier [113] is that they can be used for the simultaneous enantioanalysis of both S and R-limonen enantiomers in the same run, with higher sensitivities. The GC/MS method proposed earlier [141] for the assay of limonene is not able to discriminate between the two enantiomers.

4.2.4. Enantioanalysis of the limonene in beverages

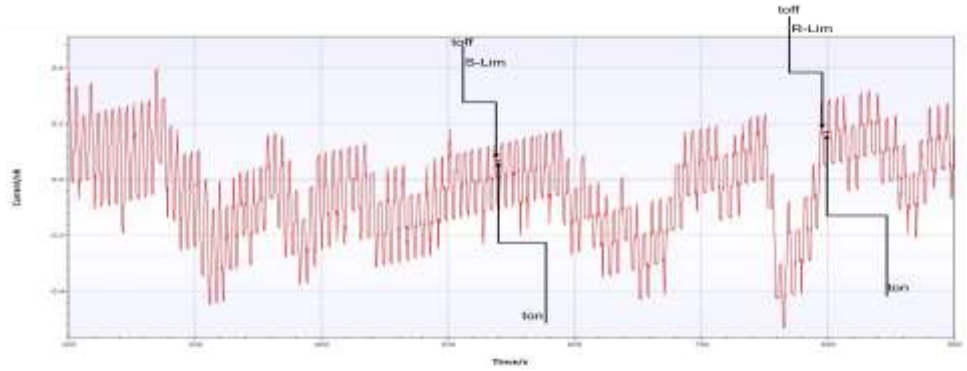
Two samples from beverages category (limoncello and triple sec liqueur) where selected for the enantioanalysis of limonene. After the recording of the diagrams (Figure 4.13), the signals of the enantiomers were identified accordingly with their signatures (t_{off} value, Table 4.8.) In between two t_{off} values, the t_{on} was read, and using the stochastic method described above, the concentration of each enantiomer was determined from the equation of calibration.



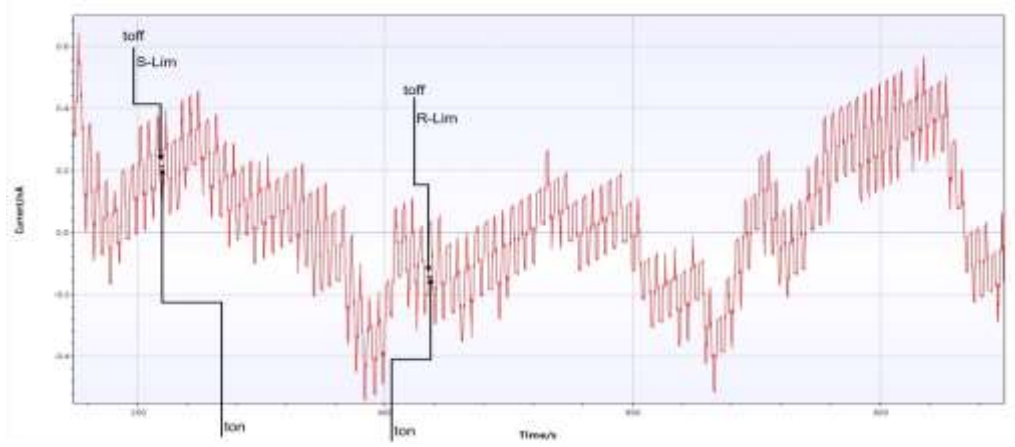
(a)



(b)



(c)



(d)

Figure 4.13 Examples of diagrams recorded for the enantioanalysis of limonene (Lim) when the stochastic enantioselective microsensor based on [Fe(TPFPP)]Cl was used for the screening of (a) limoncello, and (b) triple sec liqueur, and when the stochastic enantioselective microsensor based on TPP was used for the screening of (c) limoncello, and (d) triple sec liqueur.

The validation of the enantioanalysis of limonene was done by determination of the enantiomers in two beverages: limoncello, and triple sec liqueur, when paired-t-test was employed (Table 4.10), and by standard addition method when S- and R-limonene were added in different ratios to the limoncello (Table 4. 11.).

Table 4.10. Enantioanalysis of limonene in beverages using the stochastic enantioselective microsensors (N=10).

Beverage	Stochastic microsensor based on	S-Limonene (μmol L^{-1})	D-Limonene (μmol L^{-1})
Limoncello	TPP/Gr	6.91±0.02	11.91±0.03
	[Fe(TPFPP)]Cl/ Gr	6.90±0.03	11.73±0.05
Triple sec liqueur	TPP/Gr	6.89±0.03	24.63±0.04
	[Fe(TPFPP)]Cl/ Gr	6.22±0.01	23.98±0.03
t-test		1.94	2.34

A good correlation between the results obtained using both microsensors is observed (Table 4.10.). Paired t-test was also performed at 99.00% confidence level (tabulated theoretical t-value: 4.032) for each enantiomer. All calculated t-values were less than the tabulated value, proving that there is no statistically significant difference between the results obtained using the two stochastic microsensors (Table 4.10.). Accordingly, the proposed stochastic enantioselective microsensors can be reliably used for the enantioanalysis of limonene in beverages.

Table 4.11. Determination of S/R-limonene in spiked limoncello samples (N=10).

S:R	TTP-based stochastic microsensor		[Fe(TPFPP)]-based stochastic Microsensor	
	%, Recovery			
	S	R	S	R
1:1	99.65±0.03	99.40±0.02	99.84±0.02	99.37±0.03
1:2	99.41±0.01	99.53±0.03	99.74±0.03	99.61±0.02
1:10	99.51±0.02	99.84±0.01	99.64±0.02	99.93±0.01
2:1	99.76±0.03	99.57±0.01	99.95±0.01	99.72±0.03
10:1	99.65±0.02	99.88±0.01	99.63±0.01	99.94±0.02

The recoveries of S-, and R-limonene when limoncello was spiked with different ratios of S-, and R-limonene (Table 4.11) were higher than 99.00% proving again the reliability of the method. Further, the RSD% values were all lower than 0.10% proving the accuracy of determinations.

CHAPTER 5

Determination of atrazine using voltametric and stochastic sensors

5.1.3.Results and discussions

5.1.3.1. Characteristic response of the proposed electrochemical sensor

Differential pulse voltammetry (DPV) technique was used to determine the response characteristics of the electrochemical sensor. The voltammograms used for the calibration of the proposed sensor when used for the assay of atrazine, were shown in Figure 5.1. Figure 5.2. shows the calibration graph for atrazine. The working concentration range of the electrochemical sensor was between 1×10^{-8} mol L^{-1} and 1×10^{-5} mol L^{-1}, the limit of determination was 1×10^{-8} mol L^{-1}, while the limit of detection was 3×10^{-9} mol L^{-1}. The equation of calibration was:

$$I = 0.01 + 178.10 \times C_{atrazine} \quad (1)$$

where I is the current recorded in A, $C_{atrazine}$ is the concentration of atrazine in mol L^{-1}. The correlation coefficient obtained for the equation of calibration is 0.9949. The sensitivity recorded (178.1 A mol^{-1} L) is very high allowing excellent concentration differentiation.

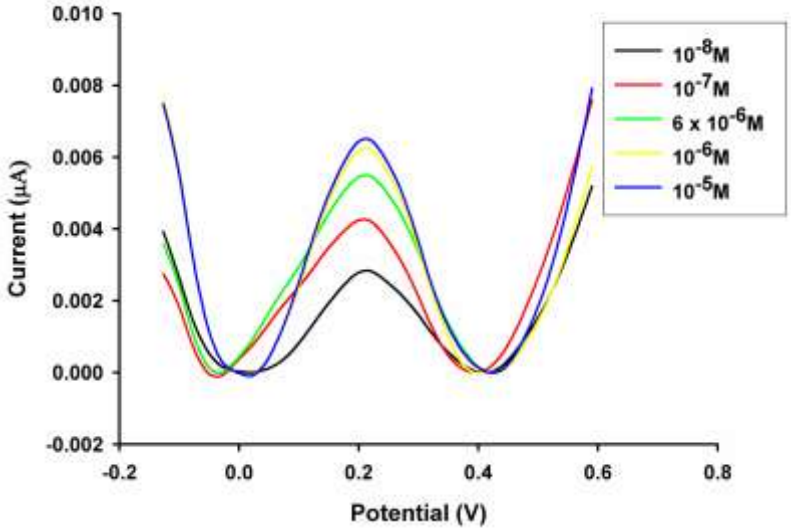


Figure 5.1. Differential pulse voltammograms obtained for different concentrations of atrazine, when a scan rate of 25 m s^{-1}, and modulation amplitude of 25 mV were used.

5.1.4. Determination of atrazine in water and beverages samples

Differential pulse voltammetry was used for the determination of atrazine whole two water samples. The electrochemical cell containing the three electrodes was immersed in the cell which was filled with the sample (water, beverages). The results of the measurements are presented in Table 5.2.

Atrazine was first determined from water samples/beverages and then known amounts of atrazine were added. The differences between the amounts of atrazine found after addition of known amounts and the initial value were compared with the added amount. The recovery test shows a high recovery of atrazine, and low RSD values.

Table 5.2. Determination of atrazine in water samples and beverages using the proposed electrochemical sensor and HPLC based methods [159] (N=10).

Samples	Amount of atrazine added (mol L^{-1})	Amount of atrazine found using the electrochemical sensors (mol L^{-1})	%, Recovery obtained when the electrochemical sensor was used	Amount of atrazine found using the HPLC method [2] (mol L^{-1})
Surface water	1×10^{-6}	9.89×10^{-7}	98.91±4.50	9.67×10^{-7}
Waste water		9.73×10^{-7}	97.27±3.99	1.02×10^{-6}
Apple flavoured drink		9.95×10^{-7}	99.48±1.86	9.78×10^{-7}
Apple juice		1.00×10^{-6}	100.20±5.31	1.04×10^{-6}
Student -t-test				1.79

A student paired-t-tests was used to compare the results obtained with the proposed electrochemical sensor, and the results obtained with the HPLC method developed by Jacomini et al. [159]. The 99.00% level of confidence (tabulated theoretical t-value: 4.032) was considered for the t-test. The values obtained (1.79) is less than the tabulated theoretical value, proving that there is no statistically significant difference in the results obtained using the electrochemical sensor and the HPLC method. Accordingly, the atrazine can be determined in fruits, and beverages accurately using the proposed electrochemical sensor.

5.2. Ultrasensitive assay of atrazine in food and water samples using stochastic sensors [165]

5.2.2.2.Design of stochastic platform

Design of the on-site screening platforms is made as following: 100 mg of graphite paste (formed from graphite powder and paraffin oil) and 100 µL solution of 4-tert-butylcalix [4] arene (1 x 10^{-3} mol L^{-1} in DMSO) for the S1 platform, and with 100 µL solution of calix[4]arene-25,26,27,28-tetrol (1 × 10^{-3} mol L^{-1} in DMSO), for the S2 platform, respectively. were added to the bare paste to give the S1 stochastic microsensor based on of 4-tert-butylcalix [4] arene and S2.

The modified pastes were introduced in the 3D plastic tube (with internal diameter of 10 µm) intersted in a 3D printed platform (Figure 5.3.), where also the reference electrode (Ag/AgCl electrode), and the counter electrode (platinum wire) were inserted.

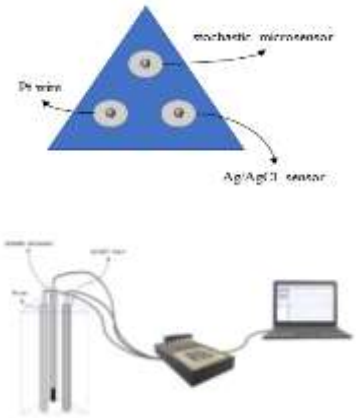
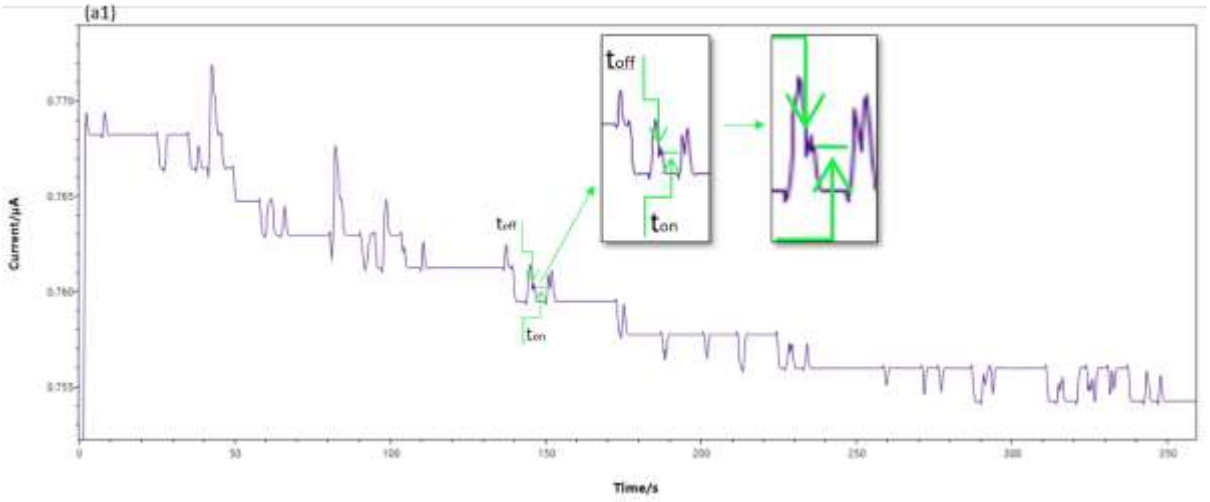


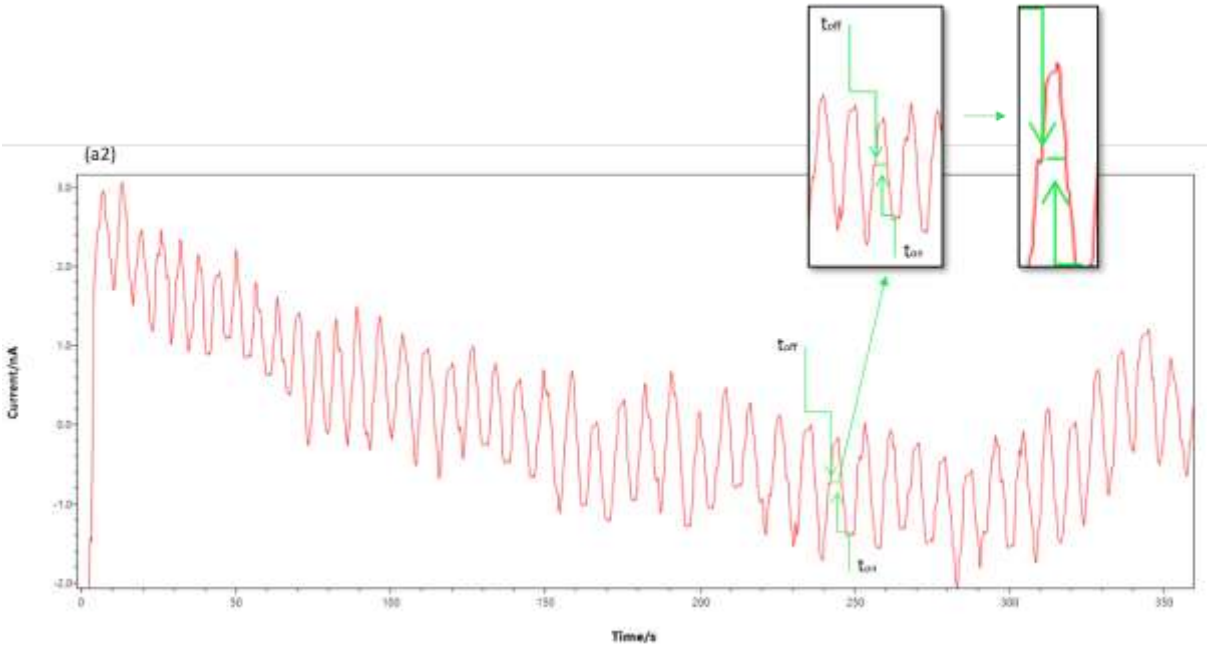
Figure 5.3. Schematic representation of the on-site screening platform, and front view of its active side.

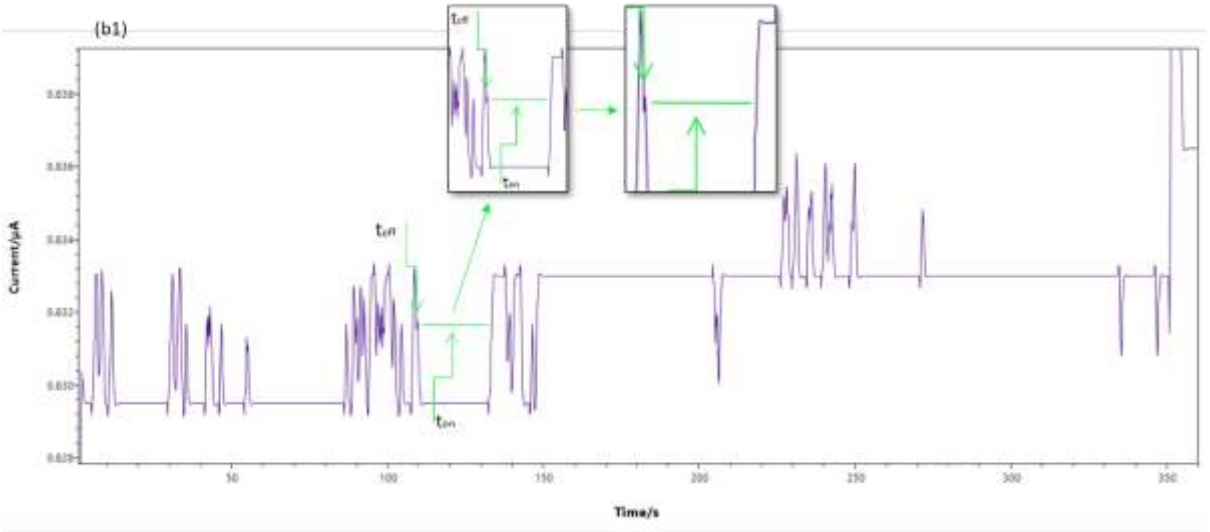
An EmSTAT Pico potentiostat (PalmSens, Houten, The Netherlands) was connected to a PC running PSTrace 5.9 to conduct all measurements. This potentiostat is able to send the diagrams, and results of the measurements via wireless to a smartphone, a laptop or a specialised database.

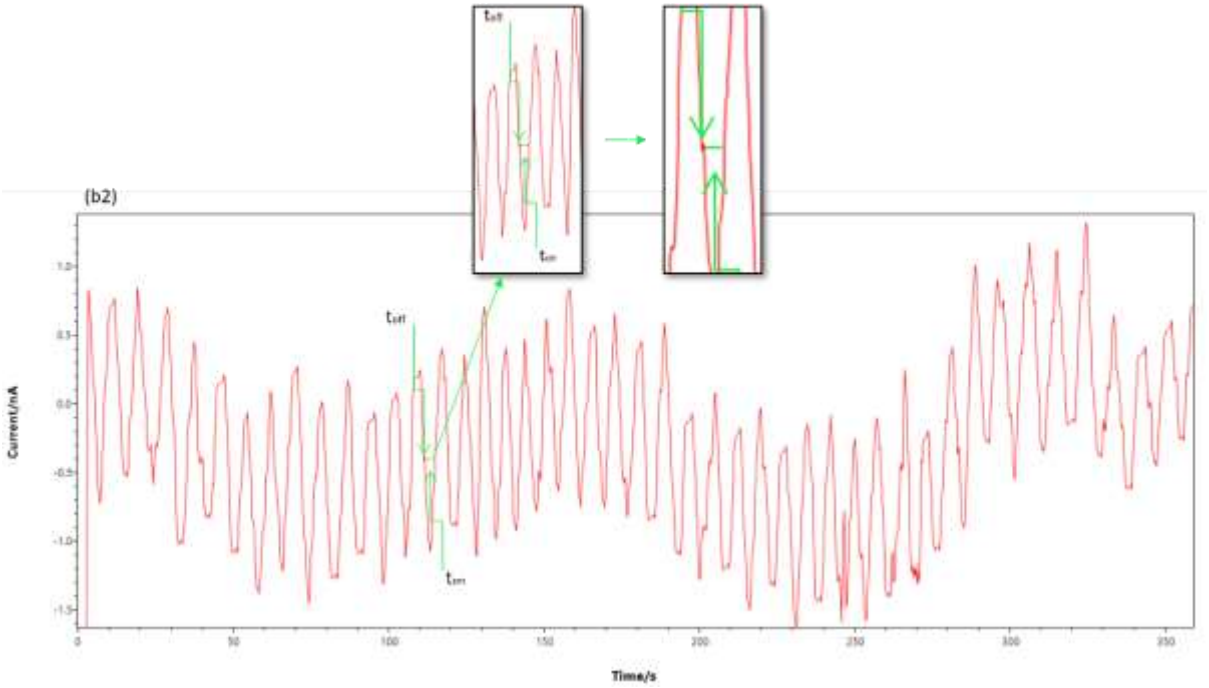
Atrazine determination using the on-site screening platform required the preparation of solutions with concentrations ranging from 10^{-18} to 10^{-3} mol/L to ascertain the response characteristics of the sensors. All measurements were performed after applying a potential of 115 mV; this potential was optimized so that the signature (t_{off} value) should be reliable read (for a higher value signatures of ns were obtained, while for lower values no signals were recorded). In the diagrams obtained, the t_{off} and t_{on} values were analyzed (Figure 5.4.).

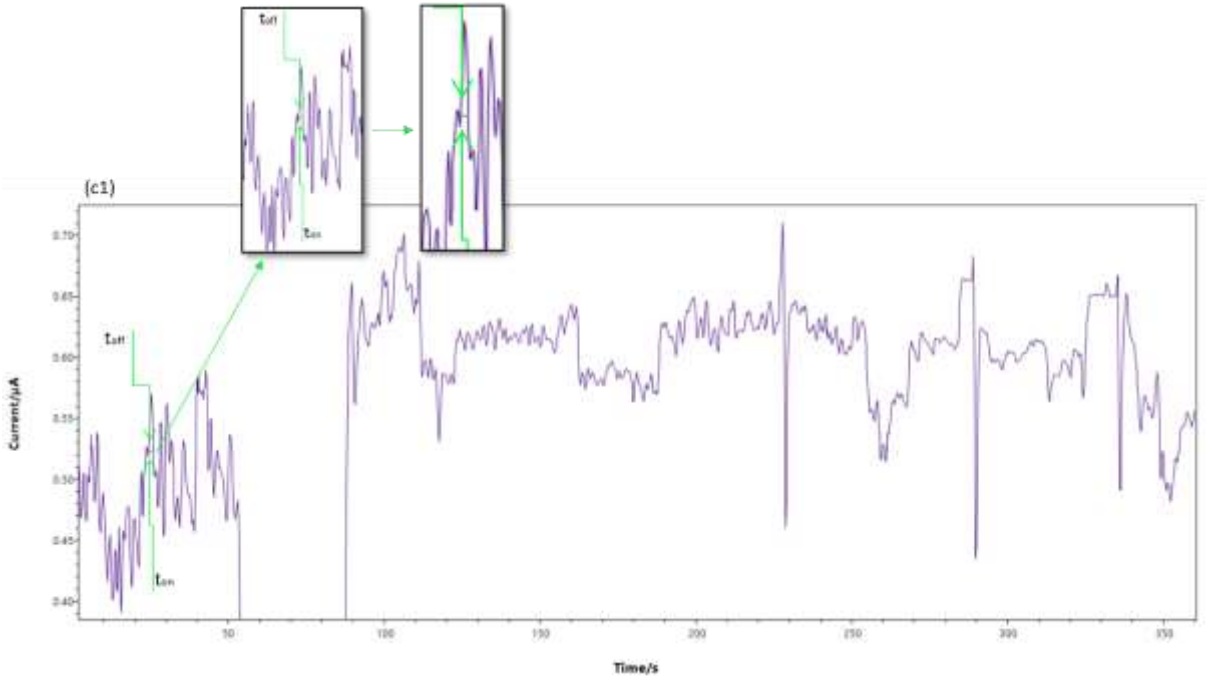
First, the signature of atrazine (t_{off} value) was identified. The second step was to read the corresponding t_{on} value (in between two t_{off} values), and use it for the determination of the equations of calibration, linear/working concentration ranges, and limits of determination. Calibration equations were determined using the linear regresion method.

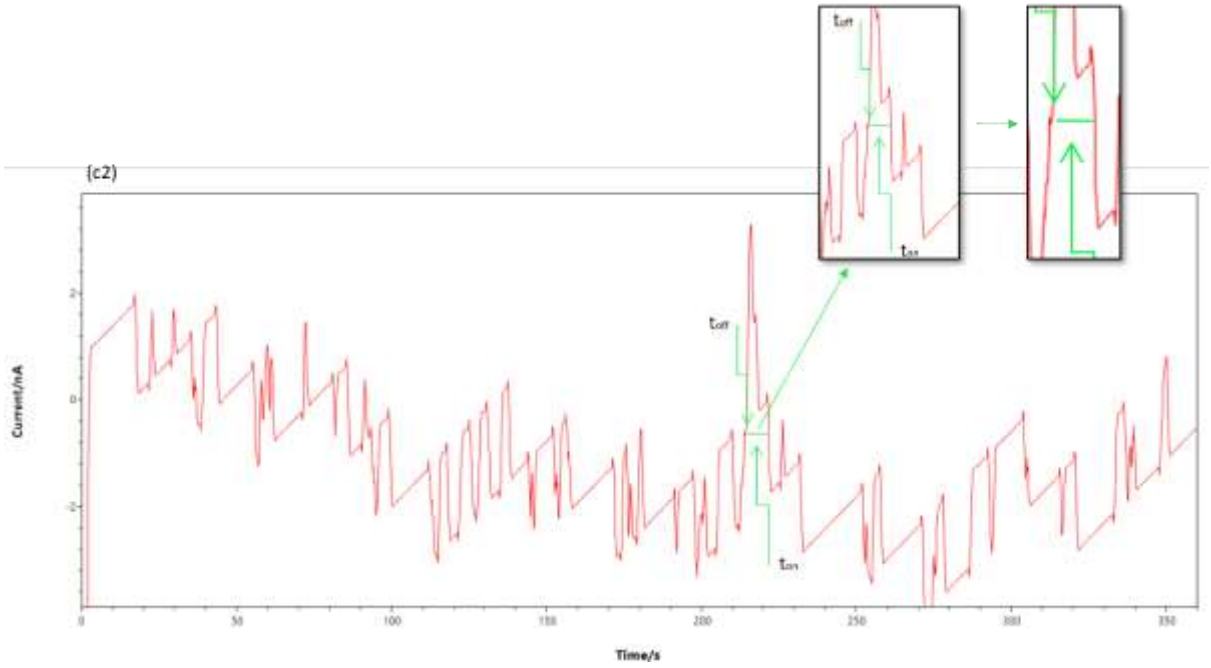


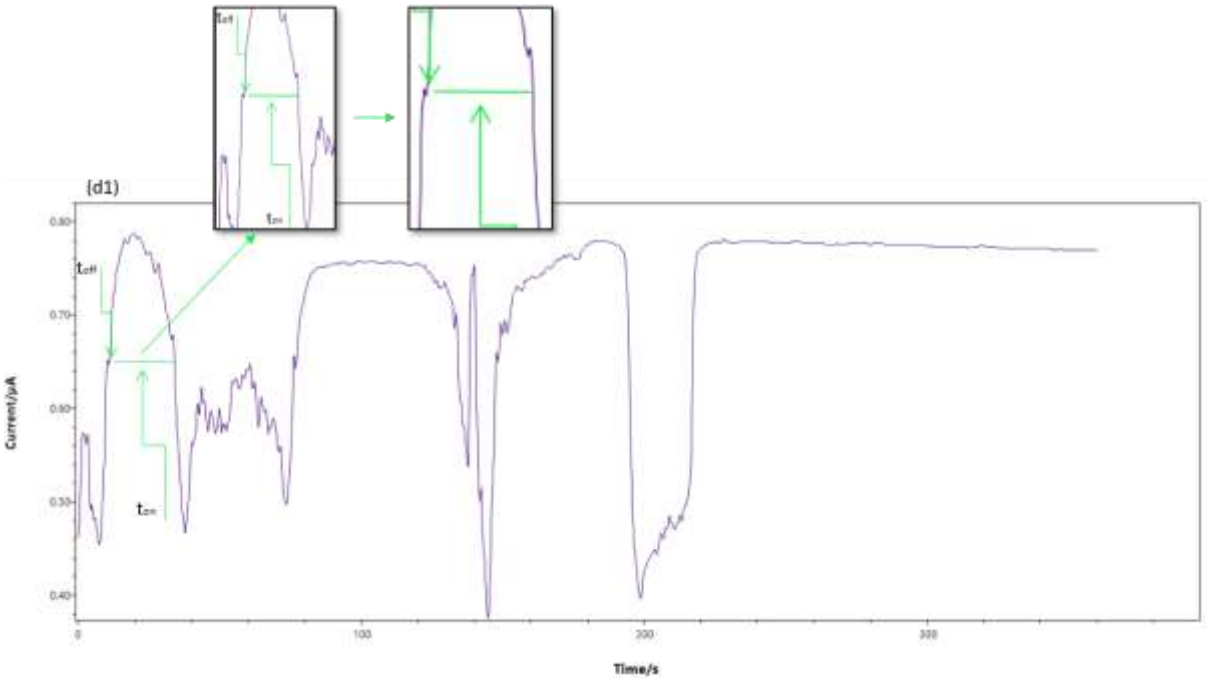

(a2)
Current/nA
Time/s


(b1)
Current/μA
Time/s


(b2)
Current/nA
Time/s


(c1)
Current/μA
Time/s


(c2)
Current/nA
Time/s


(d1)
Current/μA
Time/s

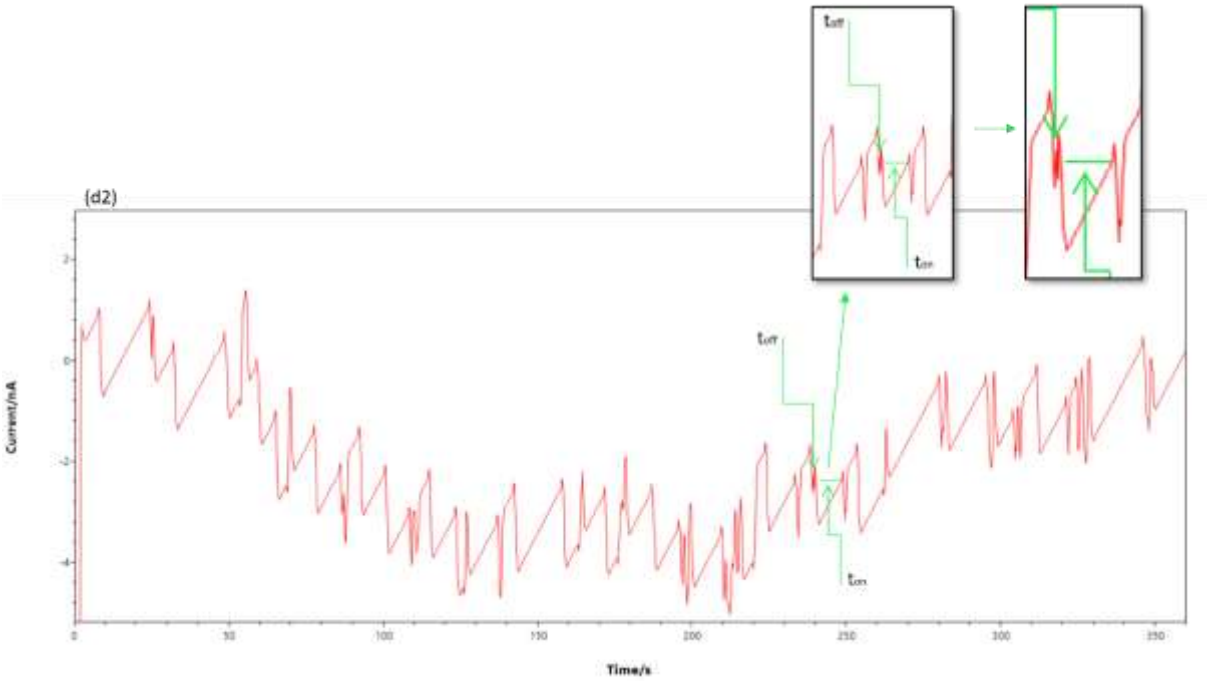


Figure 5.4. Examples of diagrams obtained using the on-site screening platforms for the assay of atrazine in (a) water samples using platforms S1 (a1) and S2 (a2); (b) in lemon using platforms S1 (b1) and S2 (b2); (c) apple using platforms S1(c1) and S2 (c2), and in (d) tomatoes using platforms S1(d1) and S2 (d2).

To qualitatively examine atrazine, we used the signature (t_{off} value) identified in the subsequent diagram. The unknown concentrations of atrazine in fruit, vegetables and water samples were determined from the calibration equation $1/t_{on} = a + bxC_{atrazine}$ recorded with each of the sensors for the atrazine. Each sensor's calibration equation was then used to calculate the unknown atrazine concentrations by reading the measured t_{on} value from the diagrams.

5.2.3. Results and discussions

5.2.3.1. Response characteristics of on-site screening platforms

Stochastic sensing principle used by the stochastic sensors incorporated into the on-site screening platforms, relies on the conductivity of a channel, with two phases: the first phase called usually the molecular recognition phase or qualitative analysis phase, in which the atrazine passes through the channel and blocks it (the time at which the channel is blocked is known as t_{off}, and its value provides information about the signature of the analyte), and the second phase known as quantitative phase, in which the analyte binds to the channel wall and promotes electrochemical processes known as quantitative phase.

The binding process taking place inside the channel, during the second phase can be briefly described using the reaction:

Ch(i) + Atrazine(i) ⇔ Ch - Atrazine(i)

where Ch is the channel, and i is the membrane-solution interface. This process is followed by the oxidation process.

Table 5.3. Response characteristics of the on-site screening platforms used for the assay of atrazine.

On-site screening platform	Working concentration range (mol L^{-1})	Calibration equation and r*	t_{off} (s)	Sensitivity (s^{-1}/ mol L^{-1})	Limit of determination (mol L^{-1})
S1	10^{-16}-10^{-4}	$1/t_{on} = 0.20 + 1.05 \times 10^{14}$ C; r=0.9986	0.4	1.05×10^{14}	1×10^{-16}
S2	10^{-16}-10^{-5}	$1/t_{on} = 1.22 + 2.11 \times 10^{14}$ C; r=0.9999	0.5	2.11×10^{14}	1×10^{-16}

* $<t_{on}>$ = s; <C> = mol L^{-1} is the concentration of atrazine; r is the correlation coefficient related to the equation of calibration.

Table 5.3. displays the signatures (t_{off} values) of atrazine which are used for the atrazine molecular recognition in different samples like fruit, vegetables, and water. The linear concentration range, sensitivity, and limits of determination were determined using the t_{on} values.

The limits of determination recorded were of 0.1 fmol L^{-1}, meaning that the sensors may be used for the ultratrace assay of atrazine in different samples. High sensitivities were obtained for each of the platforms, with the highest value obtained when the S2 platform was used. Wide linear concentration range will allow the detection of atrazine from 0.1 fmol × L^{-1} to 10 μmol x L^{-1}; this is very important, because very small amounts of atrazine may be accumulated and at a certain stage can exceed the limits set up by goverments or European Commission, as limits above which the health of the people consuming the water, fruits, and vegetables is in danger. The sensitivity of the S2 platform was higher than that of the S1 platform, proving that the -OH groups impoved the stochastic sensor's sensitivity; a higher sensitivity will make possible a better discrimination between closed concentrations of atrazine, improving the accuracy and reliability of the measurements.

Lately, the following sensors were proposed for the determination of atrazine in various samples: photoelectrochemical sensors based on an aptasensor based on CoN/g – C_3N_4 donor – acceptor configuration [160] and on Au NPs/3DOMTiO_2 photonic crystal [161], optical fiber chemiluminescent biosensor [162], electrochemical sensor based on MnO_2 –

NiO nanocatalyst [163], and a portable self-powdered sensors based on ultrasonically dispersed graphene as an electron transfer promoter [164].

Comparing the linear concentration ranges and the limits of determination obtained using the on-site screening platform with those obtained using these latest sensors proposed for the assay of atrazine: photoelectrochemical sensors based on an aptasensor based on CoN/g – C_3N_4 donor – acceptor configuration (linear concentration range between 1×10^{-4} – 10 fmol L^{-1} with limit of determination of 1×10^{-4} fmol L^{-1}) [160] and on Au NPs/3DOMTiO_2 photonic crystal (up to 167 pg L^{-1}) [161], optical fiber chemiluminescent biosensor (1 – 100 μg L^{-1}) [162], electrochemical sensor based on MnO_2 – NiO nanocatalyst (8×10^{-7} – 1.2×10^{-4} mol L^{-1}) [163], and a portable self-powdered sensors based on ultrasonically dispersed graphene as an electron transfer promoter (0.5 pmol L^{-1} - 100 nmol L^{-1}) [164], both proposed on-site screening platforms presented wider linear concentration ranges, and also the limits of determinations are lower than those reported to date.

The construction of the proposed platforms is more cost-effective, and the proposed platforms can also perform reliable molecular recognition of atrazine in food and water samples. Higher sensitivities were also recorded for the proposed platforms.

The stability of the proposed on-site screening platform in time was determined by measuring the sensitivity of the on-site screening platform during one month period of time. The results of measurements shown a variation of sensitivity in time, as following: for the S1 on-site screening platform, a variation of 0.54% was obtained, while for the S2 on-site screening platform, a variation of 0.76% was obtained; these values proved that both on-site screening platform are stable during one month, when used dayly for measurements.

Ten platforms of each type were designed and used for the assay of atrazine. For each type of platform, the sensitivities recorded were compared. A %, RSD value of 0.07 was found for the platform S1, and a %, RSD value of 0.08 was found for the platform S2. These values proved the reliability of the design of the on-site platforms based on stochastic microsensors.

5.2.4. Determination of atrazine in fruits, vegetables and water samples

The screening for atrazine in fruits, vegetables and water samples was carried out using the on-site platforms S1 and S2. The water, and the juice from fruits and vegetables

Six minutes after applying a 115 mV potential to the system, the diagrams were obtained. The atrazine was recognized in the diagrams recorded (Figure 5.4.) based on their signatures (Table 5.5.). The concentration of atrazine was calculated using the t_{on} values,

and the equations of calibration (Table 5.3.), using the procedure desctibed above. The results obtained for the determination of atrazine in different water samples, and in pieces of apple, lemon, and tomato are shown in Table 5.5. To be able to validate the method using the on-site screening platforms, a HPLC [159] method was used for comparison of the results obtained for the concentration of atrazine.

Table 5.5. Determination of atrazine in fruits, vegetables and water samples using the proposed on-site screening platforms anad the HPLC [16] method described by Jacomini et al. (N=10)

Sample No	**On-site screening platform/HPLC**	**Atrazine pmol L^{-1}**
Surface water	S1	948.00±0.02
	S2	949.03±0.03
	HPLC	947.97±0.43
Bottle water	S1	232.01±0.01
	S2	235.47±0.02
	HPLC	236.08±0.21
Waste water	S1	6430.02±0.01
	S2	6425.97±0.03
	HPLC	6426.07±0.22
Lemon juice	S1	354.03±0.02
	S2	355.00±0.05
	HPLC	353.96±0.43
Apple juice	S1	878.12±0.02
	S2	875.03±0.02
	HPLC	877.54±0.38
Tomato juice	S1	599.47±0.01
	S2	603.20±0.04
	HPLC	601.38±0.57
Student t-test for S1		2.47
Student t-test for S2		2.59

HPLC method was used as described by Jacomini et al.[159]

Student paired-t-tests were used to compare the results obtained with the two on-site screening platforms S1, and S2 with the HPLC method developed by Jacomini et al. [159]. The 99.00% level of confidence (tabulated theoretical t-value: 4.032) was considered for the t-tests. The values obtained for both platforms were less than the tabulated theoretical

value, proving that there is no statistically significant difference in the results obtained using the two platforms and the HPLC method. Accordingly, the atrazine can be determined in fruits, vegetables accurately using the on-site screening platforms.

Recovery tests were also performed after spiking the water samples and fruits with known amounts of atrazine. Results are shown in Table 5.6.

Table 5.6. Recovery tests for the assay of atrazine in water, fruits, and vegetables (N=10).

On-site screening platform	Recovery %	
	S1	S2
Surface water	99.45±0.02	99.50±0.03
Bottle water	99.97±0.03	99.90±0.02
Waste water	95.84±0.02	95.96±0.03
Lemon juice	97.13±0.01	97.27±0.02
Apple juice	98.30±0.02	98.37±0.01
Tomato juice	98.48±0.01	98.15±0.04

High values were recorded for the recovery tests proving the accuracy of the measurements. The high reliability was given by the low %, RSD values determined (Table 5.6.). This second validation test proved again that the proposed on-site screening platforms can be reliable used for the assay of atrazine in water, lemon, apple, and tomatoes.

While a good correlation between the results obtained using both the on-site screening platform, and the HPLC, the two platforms proposed for the assay of atrazine can be used on a wider working concentration range, for on-site analysis of atrazine, without any pretreatment of the samples, and they are cost-effective instruments. Given the importance of determination of such pesticide, demonstrated previously [164, 197-201], the proposed screening method for atrazine determination, which will be able to be used for more than 100 times continuously for screening of food/water samples may be used for the food and water security screenings (with high accuracy, and reliability (RSD, % values being lower than 1.00%)) in order to avoid the effects of atrazine on the health of population.

CHAPTER 6

Ultrasensitive and fast determination of ß-carotene in vegetables using stochastic sensors [202]

6.2.2. Design of stochastic sensor

For the design of the stochastic sensor, 50 mg of carbon nanopowder were mixed with 10µL of paraffin oil to form the nanocarbon paste to which 50 µL solution of calix [4] arene (1 x 10^{-3} mol L^{-1} prepared in DMSO) were added to give the modified nanocarbon paste. The contact between the modified paste and external circuit was done using a Ag wire. The paste was placed in the 3D printed tube (Figure 6.1.).

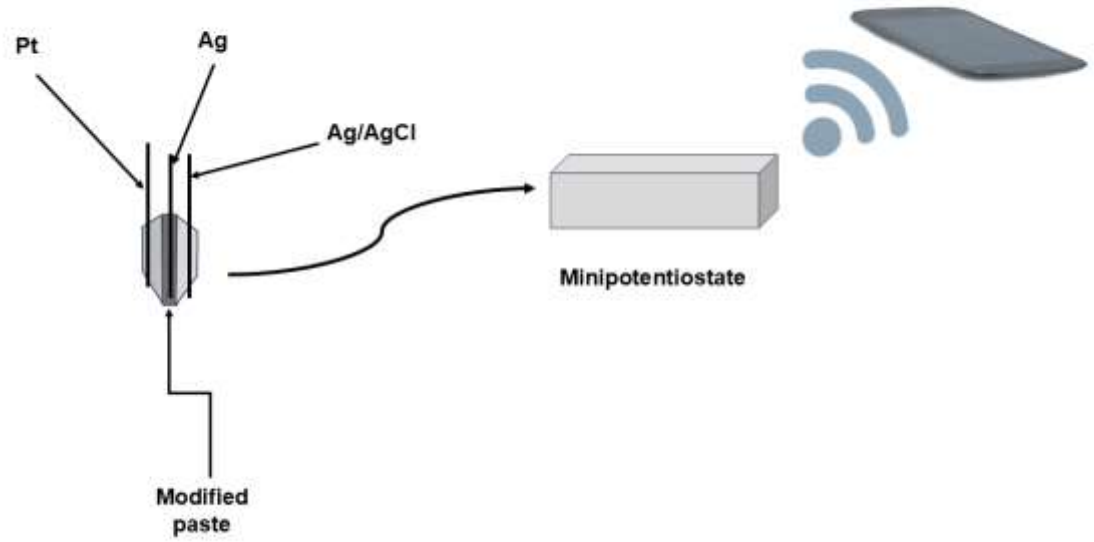
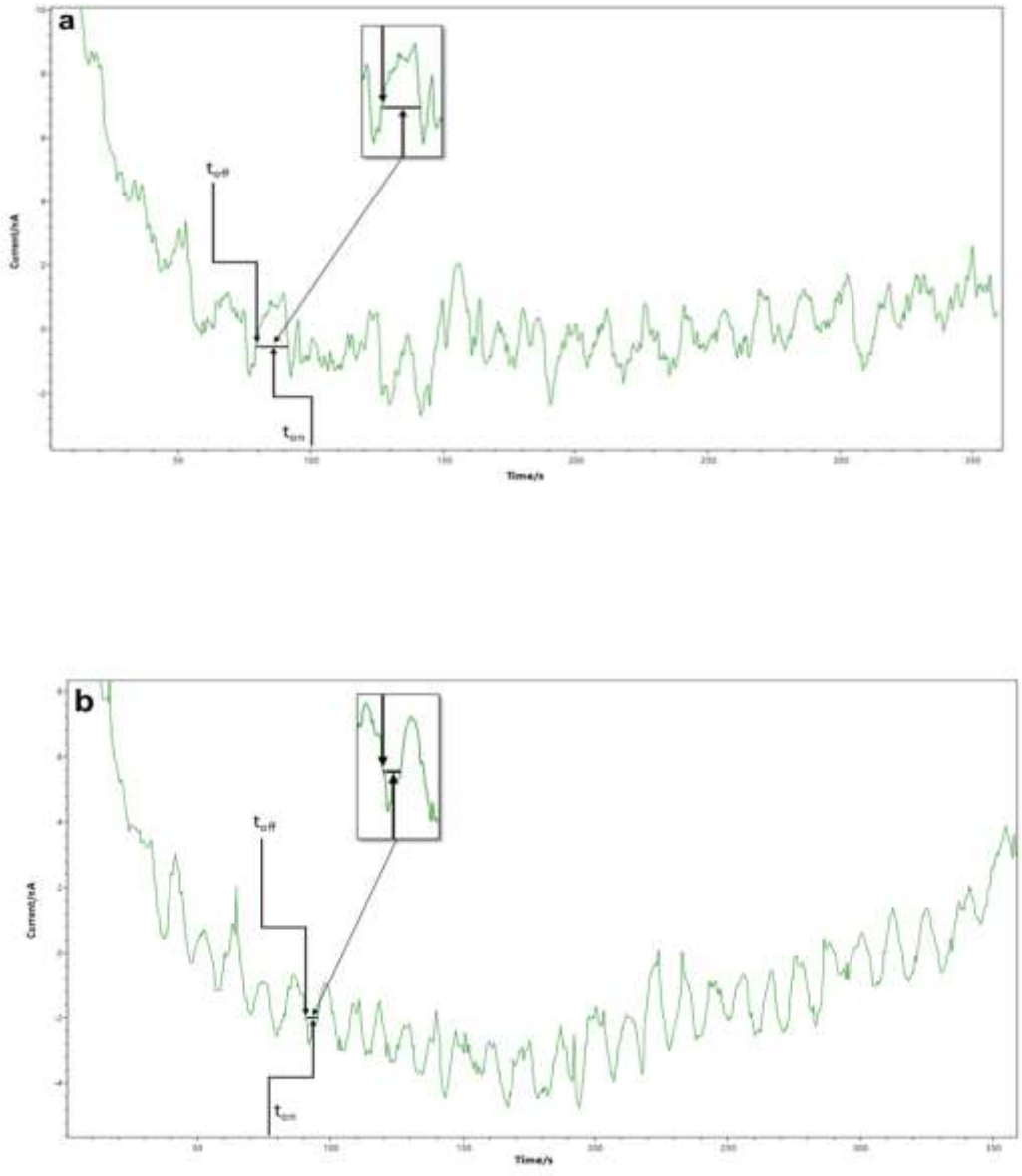


Figure 6.1. Transversal view of the 3D stochastic sensor, and schematic view of operation mode.

The internal diameter of the working electrode was 5 µm. An EmSTAT Pico potentiostat (PalmSens, Houten, The Netherlands) was connected to a PC running PSTrace 5.9 to conduct all measurements. This potentiostat is able to send the diagrams, and results of the measurements via wireless to a smartphone, and further to a specialised database.

A potential of 125 mV was applied when the ß-carotene was entering the channel, blocking it while the intensity of the current became 0 (the time needed to enter the channel is called the signature of ß-carotene, and it is read in the diagram as t_{off}). In the second stage, inside the channel there are redox processes involved during a certain period of time called t_{on}, measured in the diagram in between two consecutive t_{off} values (Figure 6.2.). A linear regression method was used to determine the parameters of the equation of calibration, while this equation was used for the determination of the concentration of ß-carotene in bell peppers, sweet potato, and orange.



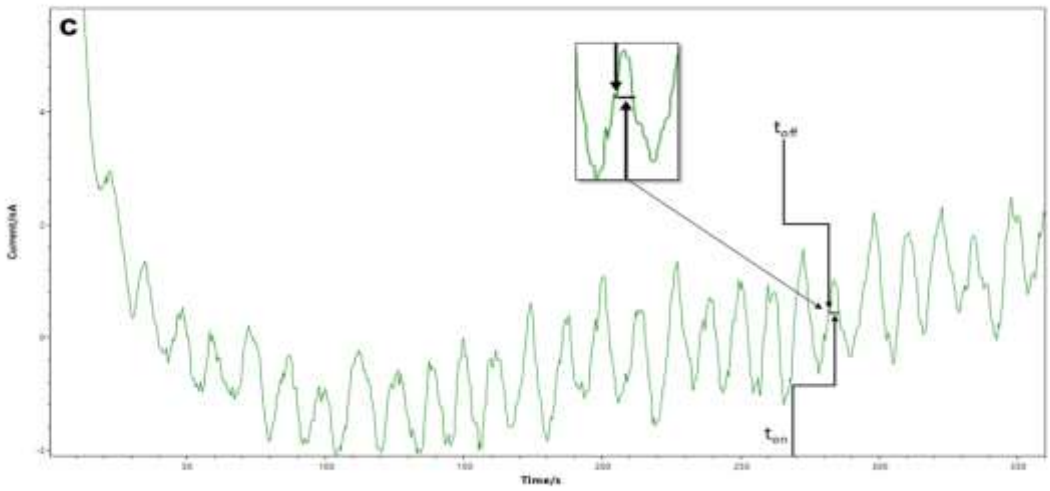


Figure 6.2. Diagrams obtained after the screening of the (a) bell peppers; (b) sweet potato, and (c) oranges with the stochastic sensor.

6.3. Results and discussions

6.3.1. Response parameters of the stochastic 3D sensor.

The response parameters of the proposed 3D stochastic sensor are shown in Table 6.1.

Table 6.1. Response parameters of the 3D stochastic sensor used for the assay of ß-carotene.

Working concentration range (mol L^{-1})	**Calibration equation and r***	**Signature t_{off} (s)**	**Sensitivity (s^{-1}/ mol L^{-1})**	**Limit of determination (mol L^{-1})**
1×10^{-17}- 1×10^{-4}	$1/t_{on} = 1.14 + 1.39 \times 10^5$ C; r=0.9991	0.7	1.39×10^5	1×10^{-17}

* $<t_{on}>$ = s; <C> = mol L^{-1} is the concentration of ß-carotene; r is the correlation coefficient for the equation of calibration.

The signature value is 0.7 s; this value is used for the qualitative analysis of ß-carotene in the samples (Figure 6.2.). The sensitivity of the proposed sensor is high over a wide linear concentration range: 1×10^{-17}- 1×10^{-4} mol L^{-1}. A limit of determination of 10 amol L^{-1} can be achieved by utilization of this sensor for the assay of ß-carotene.

Ten 3D stochastic sensors were designed as described above.

The reliability of the design of the 3D stochastic sensor was determined using the variation of the sensitivity of the ten designed 3D stochastic sensors; this variation was 0.03 % which proved a very high reliability of the design. The stability in time was determined by measuring the sensitivies of these ten sensors for 30 days, when its variation was 0.21 %, proving a good stability in time.

Compared with the methods developed earlier [207-212], the limit of the determination of the proposed method is lower, and the working concentration range wider.

6.4. Validation of the 3D stochastic sensor for the determination of ß-carotene in bell peppers, sweet potato, and oranges

The juice collected from red, orange, and yellow peppers, from sweet potato, and from orange was analysed without any sampling using the 3D stochastic sensor (Figure 6.1.). First of all the signature of ß-carotene was identified in the diagrams (Figure 6.2.) followed by the reading of the corresponding t_{on} value which was inserted in the equation of calibration of the 3D stochastic sensor to determine the concentration of ß-carotene. The results obtained using the proposed 3D stochastic sensor were compared with those obtained using the HPLC method of analysis proposed earlier, following the procedure proposed by the authors [209]. The results are shown in Table 6.2.

Table 6.2. Determination of ß-carotene in bell peppers, sweet potato, and orange using the proposed 3D stochastic sensor, and the HPLC method [209]. (N=10)

Sample	**Stochastic method/HPLC**	**ß-Carotene µg/100g**
Red bell peppers	3D Stochastic Sensor	60.00 ± 0.02
	HPLC	58.95 ± 0.49
Yellow bell peppers	3D Stochastic Sensor	100.00 ± 0.05
	HPLC	98.73 ± 0.53
Orange bell peppers	3D Stochastic Sensor	54.55 ± 0.01
	HPLC	54.12 ± 0.73
Sweet potato	3D Stochastic Sensor	55.55 ± 0.04
	HPLC	56.01 ± 0.65
Oranges	3D Stochastic Sensor	10.91 ± 0.03
	HPLC	11.03 ± 0.55
Student t-test		2.93

Student paired-t-tests were used to compare the results obtained using the HPLC [209] method and the proposed stochastic method, at 99.00 % level of confidence (tabulated theoretical t-value: 4.032). The value calculated was less than the tabulated theoretical value, proving that there is no statistically significant difference in the results obtained using the two methods. Accordingly, the proposed method can be used for the assay of ß-carotene in bell peppers, sweet potato, and oranges.

Recovery tests were also performed in order to confirm the validation of the method. The juice from the vegetables and the oranges were spiked with known amounts of ß-carotene, and after that screened using the 3D stochastic sensors. The concentrations determined using the 3D stochastic sensors were compared with those added; results are shown in Table 6.3.

Table 6.3. Recovery tests for the assay of ß-carotene in bell peppers and in oranges (N=10).

Sample	**%, Recovery**
Red bell peppers	99.45 ± 0.02
Yellow bell peppers	99.97 ± 0.03
Orange bell peppers	95.84 ± 0.02
Sweet Potato	97.13 ± 0.01
Oranges	98.30 ± 0.02

High values were recorded for the recovery of ß-carotene in different types of peppers, in sweet potato, and in oranges. These values were accompanied by very low %, RSD values, proving the accuracy and reliability of the proposed screening method used for the assessment of the concentration of ß-carotene in peppers, sweet potato, and in oranges.

Evaluation of the greenness and the method practicality and applicability are very important requirements. Accordingly, for the greenness metrics AGREE approach and software were used [218].

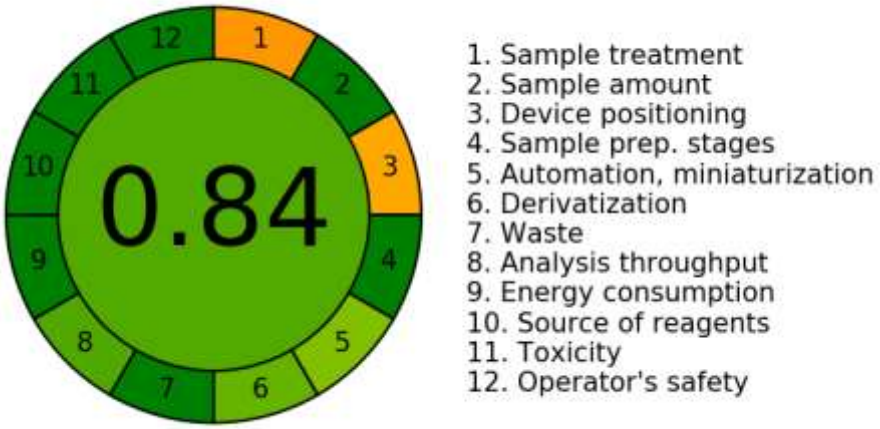


Figure 6.3. Results of AGREE analysis for the determination of ß-carotene in vegetables, when equal contribution of all criteria was considered.

In the AGREE procedure the dark green colour assigned to 1.00 value reflects the greener procedure, while light green is asigned to a green procedure that may be improved, orange colour indicates that more improved may be done, while the red colour assigned to 0 indicates that the principle or method must be changed because is not on the green line [218] (Pena-Perreira et al. 2020). The closer the value shown in the center of the circle, to 1.00, the greener the method. Twelve critera were considered by the software to attend the index of 0.84 for the greenness of the proposed method (Figure 6.3.): (1) External sample pre-treatment and batch analysis was needed; (2) 50 µL from each sample were needed for analysis; (3) the measurements were done at-line; (4) two steps were done for sample pretreatment before its analysis; (5) semi-automatic analysis was performd; (6) no derivatisation of the sample was done; (7) a maximum of 50 µL of waste was produced; (8) 40 samples h^{-1} can be analysed; (9) a very small quantity of energy was consumed as the devices are based on batteries, and the measurements are done for less than 2 min; (10) the method is reagent less; (11) no toxic reagents were used; (12) no threats were detected during or after measurements. Given the index value of 0.84 one can say that the proposed method is a green method of analysis of ß-carotene.

Blue applicability grade index (BAGI) and software [219] was used to assess the method in terms of practicality and applicability. Each score related to the software used for this assessment [219] corresponds to a colour, e.g., 10 points (the maximum number of points indicating the best scenario for the analytical method) correspond to dark blue colour, light blue colour is associated with 5.0 points, while the white colour is associated with the weaker

number of points, 2.5 points. Accordingly with the ten BAGI criteria: (1) the proposed method is quantitative and confirmatory; (2) the method was only used for the assay of one analyte – ß-carotene, (3) the method is simple in operation and it is using portable instrumentation (smartphone based detection), (4) processing of the samples is done one by one, (5) low cost of sample preparation is required, (6) 40 samples can be analysed every hour, (7) common commercially reagents were used, (8) no-preconcentration of the analytes in the samples was needed, (9) the method is semi-automated and without using commercial devices, (10) 50 µL of sample were needed for the assay of ß-carotene. Accordingly, a BAGI score of 77.50 was obtained (Figure 6.4.).



Figure 6.4. BAGI index pictogram obtained for the determination of ß-carotene in vegetables.

The final score of 77.50 points is higher than the minimum accepted value of the score (60 points), the performance of the method is high, because the final score is closed with the maximum value of the score (100 points).

CHAPTER 7

Fast screening of biological and Food Samples Using Miniplatforms Based on 3D Stochastic Microsensors [220]

7.1.1. Design of the Stochastic Sensor

100mg of nanographene powder was divided into two equal parts, and was physically mixed with 10mg of spheroidal Cu and 10mg copper oxide nanoparticles. Then, paraffin oil was added to each of the two parts, to obtain homogeneous pastes. To each part were added 50μL of solution β-cyclodextrin (10^{-3} mol L^{-1}). The silver wire was utilized as a means of establishing contact between the paste and the external circuit.

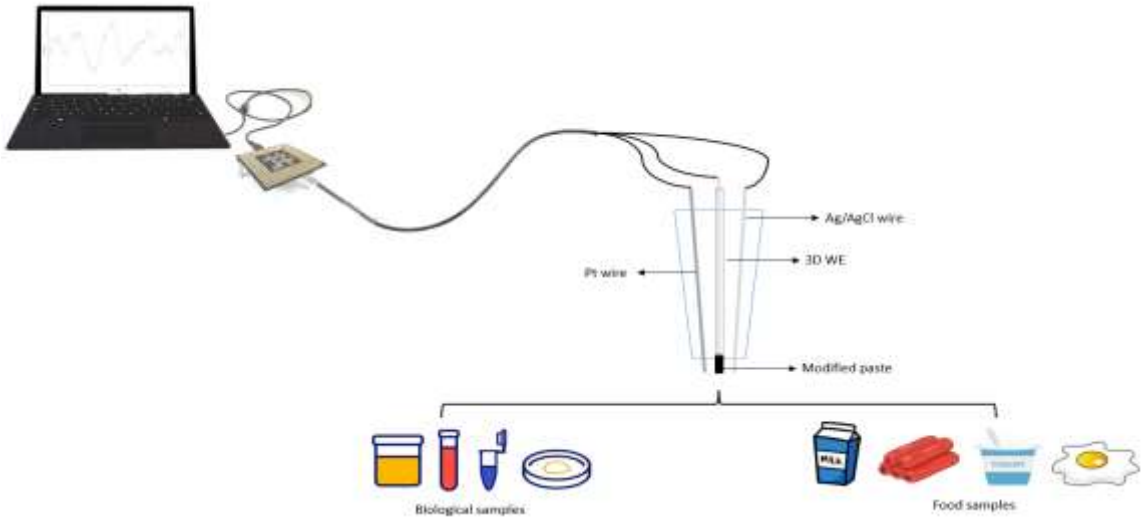


Figure 7.1. Design of the miniplatform containing the 3D stochastic microsensor, and schematic representation of the measurements.

Each modified paste was carefully inserted into a plastic tube made of a non-conducting material, with an inner diameter of 10μm. The microsensor was integrated in a miniplatform together with the reference (Ag/AgCl), and an auxiliary (Pt) electrode (Figure 7.1.).

7.2. Results and discussions

7.2.1. Response characteristics of the miniplatforms based on 3D stochastic microsensors

The stochastic microsensors' response principle is based on the conductivity of the channel. The modified paste is being subjected to a potential of 125 mV, and the biomarkers are being introduced one at a time into the pores of the active surface. During the process of entry, the pore is being partially blocked and the intensity of the current became close to 0. The amount of time that was spent on this stage is referred to as the signature of the biomarker, and the value that represents it is referred to as the t_{off} value (signature of enantiomer). The subsequent phase involves the biomarker going through binding processes as well as redox processes. The total amount of time that is spent on these processes is referred to as the t_{on}, and the enantiomer is then utilized for quantitative measurements. Table 7.1. displays the response characteristics of the miniplatforms used for the aspartic acid determination.

The results shown in Table 7.1. demonstrate that there are differences between the signatures recorded for the enantiomers of Asp when the miniplatform based on the same 3D stochastic microsensor was used; as expected the stereochemistry of the enantiomers places an important role in the time needed for the molecules of the enantiomers to enter into the channel. This demonstrates that the miniplatforms are feasible for the enantioanalysis of Asp in biological and dietary samples. The response characteristics are provided for each of the enantiomers of Asp and each of the miniplatform based on 3D stochastic microsensors in Table 7.1. These parameters include signature of the enantiomer, sensitivity, limit of determination, working concentration range, and equations of calibration. For the assay of L-Asp, the best sensitivity was recorded when the 3D stochastic microsensor βCD /Cu spher/nGr was used, while a wider working concentration range was reported for the stochastic microsensor based on βCD/CuONPs/nGr, while the limit of determination (determined accordingly with the IUPAC definition as the lowest concentration from the linear concentration range) is not dependent on the type of Cu compound used for the design of the microsensor. The βCD /Cu spher/nGr microsensor provided a broader linear concentration range for the assay of D-Asp than the other stochastic microsensors. However, the sensitivity and the lower limit of quantification that were recorded were fairly comparable for both miniplatforms. Once more, the value of the limit of quantification was not affected in any way by the type of Cu compound used in the microsensor design.

Table 7.1. The response characteristics of the miniplatforms based on3D stochastic microsensors for the enantioanalysis of aspartic acid.

Miniplatform containing the 3D stochastic microsensor based on	Asp	Signature (s)	Equation of calibration r*	Working conc. range (mol L^{-1})	Sensitivity (s^{-1} mol^{-1} L)	Limit of quantification (mol L^{-1})
βCD/CuONPs/nGr	L	0.5	$1/t_{on}$=0.81+1.72×10^6 C r= 0.9706	1×10^{-18} -1× 10^{-6}	1.72×10^6	1×10^{-18}
	D	0.7	$1/t_{on}$=0.36+1.64 × 10^8 C r= 0.9993	1×10^{-18} -1× 10^{-8}	1.64×10^8	1×10^{-18}
βCD/Cu spher/nGr	L	0.7	$1/t_{on}$=2.12+1.59× 10^{10} C r= 0.9858	1×10^{-18} -1× 10^{-7}	1.59× 10^{10}	1×10^{-18}
	D	0.5	$1/t_{on}$=2.67+6.85 × 10^8 C r= 0.9998	1×10^{-18} -1× 10^{-6}	6.85×10^8	1×10^{-18}

*<t_{on}>=s; <C>= mol L^{-1}

The reliability of the design and the stability of the miniplatforms were evaluate. Ten miniplatforms of each kind were designed as described above; their sensitivities were measured and compared; RSD% values of 1.02% and 0.98% were recorded for the mini-platforms on which 3D stochastic microsensors βCD/CuONPs/nGr, and βCD /Cu spher/nGr, respectively were used proving a high reliability of the proposed design.

For each of the miniplatform designed, the sensitivity was measured every day for a period of one month, after which the RSD% values of 1.14% and 1.20% were recorded for the miniplatforms on which 3D stochastic microsensors βCD/CuONPs/nGr, and βCD /Cu spher/nGr, proving their high stability in time.

7.3. Enantioanalysis of aspartic acid in food and biological samples

Table 7.5. Determination of aspartic acid in food samples (N=10).

Sample	Asp*	Miniplatform based on	
		βCD/CuONPs/nGr	βCD /Cu spher/nGr
Hotdog	L	984.02 ± 0.01	985.01 ± 0.03
	D	242.00 ± 0.03	241.96 ± 0.01
Milk	L	498.55 ± 0.03	498.83 ± 0.01
	D	10.01 ± 0.01	9.69 ± 0.03
Raw egg white	L	452.32± 0.04	460.12 ± 0.03
	D	2.16 ± 0.01	2.20 ± 0.01
Raw egg yolk	L	84.91 ± 0.01	85.00 ± 0.03
	D	4.58 ± 0.03	4.60 ± 0.01
Plain Yoghurt	L	984.02 ± 0.01	983.20 ± 0.04
	D	5.43 ± 0.01	5.40 ± 0.02
Yoghurt whey	L	586.82 ± 0.01	587.03 ± 0.03
	D	2.89 ± 0.03	2.80 ± 0.01

The findings presented in Tables 7.1.-7.5. demonstrate that the miniplatforms based on 3D stochastic microsensors that were constructed have the capability to accurately conduct enantioanalysis of Asp in a single run without any sample pretreatment. Their accuracy, limit of determination and sensitivity are higher than those reported to date for the analysis and enantioanalysis of Asp [228-241].

CHAPTER 8

Stochastic Determination of Ethyl Propionate in Commercial Juices

8.2.1. The design of the 3D combined stochastic sensor

100 mg reduced nanographene oxide powder were mixed with 100 μL of 0.001 mol L^{-1} solution of N-(pyridine-3-yimethyl)oleamide; this is the optimized composition as no signal was obtained when less than 100 μL of 0.001 mol L^{-1} solution of N-(pyridine-3-yimethyl)oleamide were added, and no change in the signal was obtained for volumes lower than 150 μL of 0.001 mol L^{-1} solution of N-(pyridine-3-yimethyl)oleamide, but for higher

volumes than 150 µL the signal specific for stochastic sensors was not found. 30 µL of paraffin oil were added to form the paste. The paste was placed in a 3D non-porous and non-conducting plastic printed tube (Figure 8.3.); a special printer was used for the printing of the tube used for the design of the sensor.

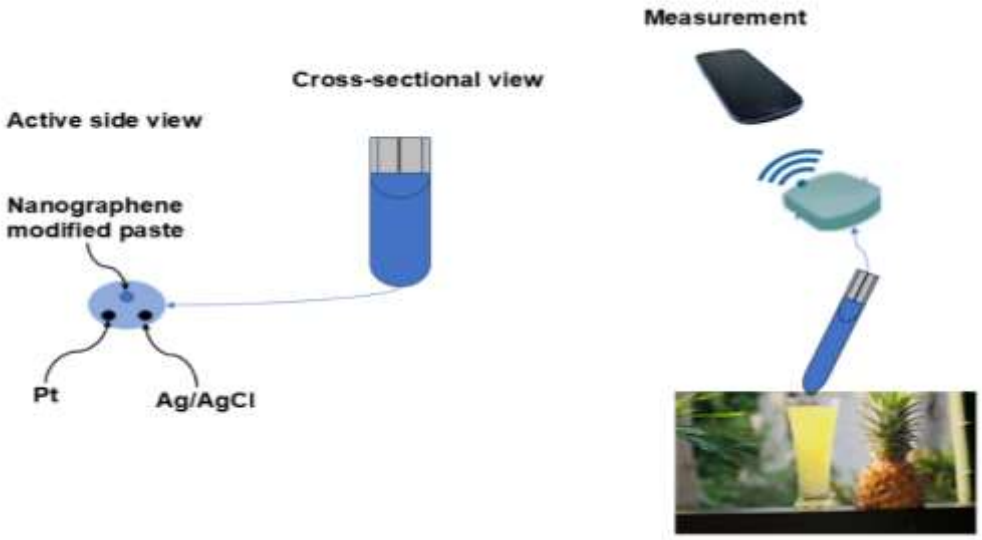


Figure 8.3. Active side view and cross-sectional view of the 3D combined stochastic sensor. A set-up of the measurement used for the determination of ethyl propionate in juice.

Connection between the paste and external circuit is done using a Ag wire. Pt and Ag/AgCl wires are also inserted into the 3D plastic tube (Figure 8.3.) to finalize the construction of 3D combined stochastic sensor.

8.3. Results and discussions

8.3.1. Response characteristics of the 3D combined stochastic sensor.

The response characteristics of the 3D combined stochastic sensor were determined using the stochastic method described above. The signature of ethyl propionate was 1.2 s. The equation of calibration obtained for the calibration of the sensor using the ethyl propionate standard solutions was $1/t_{on}=0.29+1.37\times10^{10}C_{ethyl\ propionat}$, with a correlation coefficient of 0.9999, while the calibration of the sensor using solutions of the same concentrations of ethyl propionate prepared in juice, is $1/t_{on}=0.30+1.37\times10^{10}C_{ethyl\ propionat}$, with a correlation coefficient of 0.9998. The units for t_{on} and $C_{ethyl\ propionat}$ were s, and mol L^{-1}, respectively.

There is only a small difference on the intercept of the calibration graph, proving that the matrix of the juice does not have an effect on the analysis of ethyl propionat. The graph corresponding for the calibration of the proposed sensor is shown in Figure 8.4.

The ethyl propionate can be determined on a wide linear concentration range, between 1×10^{-15} and 1×10^{-4} mol L^{-1} despite if the determination are done using standard ethyl propionate solutions or in the solutions prepared using the juice, with a sensitivity of 1.37×10^{10} s^{-1} mol^{-1} L. The working linear concentration range facilitates determination of ethyl propionate from ultra trace amounts to high amounts of ethyl propionate.

The limit of quantification of ethyl propionate is 1 fmol L^{-1} (accordingly with IUPAC recommendations, this value represents the lowest concentration from the linear concentration range, new IUPAC recommendation (paragraph 3.36, Note 3) [265]).

Table 8.1. Methods used for the determination of ethyl propionate.

Method	Linear concentration range	Limit of quantification	Reference
Gas chromatography–mass spectrometry	960.17-1231.70 μg mL^{-1}	960.17 μg mL^{-1}	[254]
Amperometry using gaseous sensors	> 1 pmol L^{-1}	1 pmol L^{-1}	[255]
This work	1×10^{-15} - 1×10^{-4} mol L^{-1}	1 fmol L^{-1}	-

Comparing the linear concentration range and the limit of quantification obtained for the proposed 3D combined stochastic sensor with those obtained using the methods proposed earlier (Table 8.1.), the wider linear concentration range, and the lowest limit of quantification were obtained when the proposed sensor was used.

The reliability of the construction of the 3D combined stochastic sensor was determined by comparing the sensitivities obtained for 20 sensors constructed using the procedure described above; a deviation of 0.08 % from the mean value of the sensitivity proved that the proposed design is reliable.

The sensitivities were continuously measured for the 20 sensors as long as 30 days; a deviation from the mean of the sensitivity of 0.09 % was recorded proving the stability of the 3D combined stochastic sensor for at least 30 days.

8.4. Validation of the 3D combined stochastic sensor.

A commercial juice was used as real sample for the sensor and screening method validation. 10 different known amounts of ethyl propionat were added to the juice. Screenings of the juice samples were performed before and after the addition of the known amounts. The determined concentration of ethyl propionate and the theoretical (calculated) concentration of ethyl propionate were compared (Table 8.3.).

Table 8.3. Recovery of ethyl propionat in juice samples using the 3D combined stochastic sensor.

Sample No.	Calculated concentration, mol L^{-1}	Determined concentration, mol L^{-1}	%, Recovery of ethyl propionat
1	7.32×10^{-14}	$7.26(\pm0.11)\times10^{-14}$	99.93±0.13
2	3.96×10^{-13}	$3.94(\pm0.10)\times10^{-14}$	99.95±0.10
3	3.70×10^{-12}	$3.69(\pm0.08)\times10^{-12}$	99.90±0.09
4	7.50×10^{-12}	$7.47(\pm0.07)\times10^{-12}$	99.67±0.08
5	2.34×10^{-11}	$2.32(\pm0.13)\times10^{-11}$	99.50±0.09
6	1.23×10^{-10}	$1.22(\pm0.11)\times10^{-10}$	99.23±0.11
7	2.50×10^{-9}	$2.49(\pm0.10)\times10^{-9}$	99.82±0.11
8	3.43×10^{-7}	$3.41(\pm0.09)\times10^{-7}$	99.46±0.12
9	1.30×10^{-6}	$1.29(\pm0.12)\times10^{-6}$	99.89±0.10
10	2.87×10^{-5}	$2.90(\pm0.12)\times10^{-5}$	101.35±0.12

The concentrations of ethyl propionate were determined as following: the first step was to identify in the diagram (Figure 8.5.) the signature (t_{off} value) of ethyl propionate.

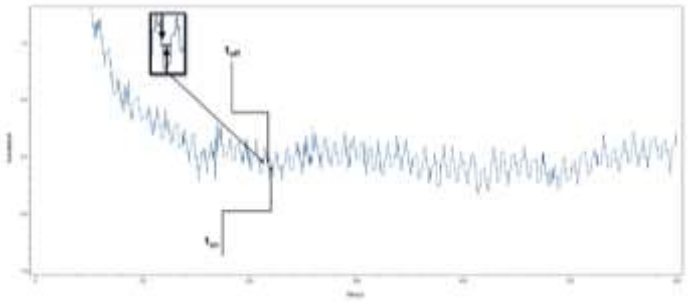


Figure 8.5. Diagram obtained while screening the juice sample for ethyl propionate using the stochastic method (he applied potential vs Ag/AgCl was 12 mV).

The second step is to read the t_{on} value just after the t_{off} value in the diagram (Figure 4-8.4.8.). After that, the stochastic method described above was applied to determine the concentration of ethyl propionate.

The average recovery of ethyl propionate in juice samples was 99.87 % and the relative standard deviation was 0.10 % (N=10). This value proved the reliability of the proposed sensor and screening method.

Comparison between the proposed method and the gas chromatography-mass spectrometry method [254] was done for three juice samples obtained from the same provider, but from different lots; the results are shown in Table 8.4.

Table 8.4. Determination of ethyl propionat in three lots of the same juice samples, obtained from the same provided (N=10).

Lot no.	Concentration of ethyl propionat, μmol L^{-1}	
	Stochastic method	Gas chromatography-mass spectrometry method [254]
1	3.87±0.08	3.50±0.43
2	2.21±0.10	2.43±0.54
3	17.75±0.12	16.97±0.46

A Student t-test at 99% confidence level was performed (tabulated value 4.13). The calculated value was 2.27, which is lower than the tabulated value proving that there is no significant difference between the results obtained using the two methods: stochastic method and the gas chromatography-mass spectrometry method, when used for the determination of ethyl propionate in juice.

Further advantages of this screening method versus the methods proposed earlier [252-255] are: no sampling is needed before the measurement/screening of the sample, high reliability is recorded.

Conclusions

General conclusions

Ultrasensitive determination of sorbic acid in food is essential for the assessment of the food quality. Therefore, two sensors based on nanographene decorated with gold nanoparticles paste modified with metal porphyrins (Zn protoporphyrin IX, and 2,3,7,8,12,13,17,18 octaethyl, 21H, 23H-porphirine Mn(III) chloride) were proposed for the determination of sorbic acid in food (bakery products and mayonnaise). Square wave voltammetry was used for the characterization and validation of the proposed sensors. Response characteristics shown that the limits of detection for both sensors were 0.33 μmol L^{-1} while the limits of quantification were 1.00 μmol L^{-1}. Both sensors can be used for the determination of sorbic acid in the concentration range 1 - 1000 μmol L^{-1}; the linear concentration range making them appropriate for the assay of sorbic acid in food. The highest sensitivity (0.35nA/μmol L^{-1}) was recorded when the sensor based on 2,3,7,8,12,13,17,18 octaethyl, 21H, 23H-porphirine Mn(III) chloride was used, proving the higher electrocatalytic effect of this electrocatalyst versus the one of the Zn protoporphyrin IX. High recoveries (values higher than 95.00%) and low RSD (%) values (lower than 5.00%) were recorded for both sensors when used for the determination of sorbic acid in bread and mayonnaise, proving the high reliability of the proposed sensors and method. The feature of the proposed sensors is their utilization in food industry and supermarkets for the quality control of food, regarding the assay of the concentration of sorbic acid.

Two sensors based on sulfur-doped graphene, gold nanoparticle paste modified with 5,10,15,20-tetraphenyl-21H,23H-porphine and 5,10,15,20-tetrakis (pentafluorophenyl chloride)-21H,23H-iron (III) porphyrin were proposed for the determination of R-limonene in beverages (triple sec liqueur and limoncello). Differential pulse voltammetry was the method used to characterize and validate the proposed sensors. The response characteristics showed that the detection limits for both sensors were 3×10^{-6} mol L^{-1}, while the quantification limits were 1×10^{-5} mol L^{-1}. Both sensors can be used to determine R-limonene in a concentration range between 1×10^{-5} - 6×10^{-4} mol L^{-1} for TPP/AuNPs-S-Gr and 1×10^{-5} - 1×10^{-3} mol L^{-1} for Fe(TPFPP)Cl/AuNPs-S-Gr. The highest sensitivity (0.7068 μA/mol L^{-1}) was recorded when the TPP/AuNPs-S-Gr sensor was used, proving that the electrocatalytic effect of this electrocatalyst is higher compared to that of Fe(TPFPP)Cl/AuNPs-S-Gr. High recoveries (values greater than 99.00%) and low RSD values (%) (below 5.00%) were recorded for both sensors when used to determine R-limonene in triple sec liqueur and limoncello. The feature

of the proposed sensors is their use in the food industry and super-markets for food quality control, in terms of R-limonene determination.

Enantioanalysis plays a very important role in different fields, including food sciences. (R)-limonene is responsible for the fragrance of the juice while the (S)-limonene's flagrance does affect the test of beverages. Enantioanalysis based on utilization of stochastic enantioselective microsensors designed using the immobilization of 5,10,15,20-tetraphenyl-21H,23H-porphine (TPP) and of 5,10,15,20-tetrakis(pentafluorophenyl)-21H,23H-porphyrin iron (III) chloride [Fe(TPFPP)]Cl in reduced graphene oxide decorated with Pd(0) and with gold nanoparticles, was performed to discriminate between the enantiomers S and R of limonene in order to determine racemization processes, and the source of the limonene. The signatures of the enantiomers are different when both microsensors were used, proving there enantioselectivity. The highest sensitivity for the assay of S-limonene was achieved by using the stochastic enantioselective microsensor based on [Fe(TPFPP)]Cl while the highest sensitivity for the assay of R-limonene was achieved when the stochastic enantioselective microsensor based on TPP was used. High reliability was achieved when the enantioanalysis of limonene was performed from different beverages. The feature of the method is its utilization for the assay of the quality of beverages regarding the presence of R/S-limonene.

A new electronalytical method based on a voltametric sensor was proposed for the assay of atrazine, which is a triazine herbicide widely used in the environment due to its water solubility and slow degradation. A voltametric sensor constructed using the physical immobilisation of 5,10,15,20-tetraphenyl-21H,23H-porphine in a nanographene paste was used for the determination of atrazine in water and in beverages. The working concentration range was between 1×10^{-8} and 1×10^{-4} mol L^{-1} with a sensitivity of 178.10 A $mol^{-1}L$. Recoveries higher than 97.00% were obtained, when the sensor was used for the assay of atrazine in water, apple flavourd drink, and apple juice. The features of the proposed electrochemical sensors are connected with its utilization as screening tool for the quality of water, as well as in supermarkets for food security checks.

An ultrasensitive assay of atrazine from fruit and water samples, using a on-site screening platforms incorporating stochastic microsensors based on graphite powder modified with 4-tert-butylcalix [4] arene and with calix [4] arene-25,26,27,28-tetrol was proposed. Limits of determination of 0.1 fmol L^{-1} were recorded while the sensors could have been used on wide concentration ranges, between 0.1 fmol L^{-1} and 0.1mmol L^{-1}.

Recoveries higher than 95.00% were recorded when used for the assay of atrazine in water, fruits and vegetables. The proposed on-site screening platforms are cost-effective. There is a great feature for the proposed on-site screening platforms – as tools for assessing the quality of water, fruits, and vegetables. By performing such screening tests, the state of health of population can be substantially improved, being proved that they can affect in different ways the state of health, being responsible for producing different illnesses in the human body.

Bell peppers, sweet potato, and oranges contain ß-carotene. An ultrasensitive stochastic sensor based on a nanocarbon paste matrix modified with calix[4]arene, coupled to a portable instrument able to send data to a smartphone operated by a special program which process data and send the quality results to a database, was developed. The sensor can be used between 10 amol L^{-1} and 0.10 mmol L^{-1}, with high sensitivity for the assay of ß-carotene in vegetables and fruits. Recoveries higher than 98.00 % were obtained when the sensor was used for the assay of ß-carotene in different types of vegetables and fruits. The proposed method is green, and performance. Its feature is the on-site ultrasensitive and fast assay of quality of sweet potato, and in oranges for food security and quality control.

A novel approach for the enantioanalysis of aspartic acid employing miniplatforms containing stochastic enantioselective sensors as detection tools was validated using food and biological samples. The 3D stochastic sensors were based on the modification with β-cyclodextrin of a functionalized copper oxide nanoparticles and spheroidal copper particles nanographene powder matrix. Stochastic method was used for all measurements. The sensors proposed demonstrated low limits of determination (1×10^{-18} mol L^{-1}), high sensitivities (the highest being recorded for the spheroidal copper particles nanographene powder matrix based sensor: 1.59×10^{10} s^{-1} mol^{-1} L for L-aspartic acid, and 6.85×10^{8} s^{-1} mol^{-1} L for D-aspartic acid), and wide linear concentration ranges (up to 12 decades of concentrations) for the enantioanalysis of aspartic acid. Student t-test values recorded were less than 3, when data obtained using both proposed sensors were compared, proving that it is no significative differences between the results obtained using the new designed sensors. Recovery values higher than 99.00% were recorded for the determination of the enantiomers of aspartic acid despite the ratio on which they are found in the synthetic mixtures. The type of Cu compound used for the active surface design did influence the sensitivity as well as the working concentration range, but did not influence the limit of determination. Validation of the miniplatforms facilitate a very important feature of the miniplatforms: their utilisation for on-site screening tests of biological samples for early diagnosis of gastric cancer, and the fast food control in supermarkets.

Ethyl propionate is a versatile compound gaining traction for its potent ability to enhance flavor. Ethyl propionate has the same flavor like pineapple. Its analysis from pineapple juice may be able to make a difference between the natural and synthetic pineapple juices. Therefore, a 3D combined stochastic sensor based on reduced nanographene oxide paste modified with N-(pyridine-3-yimethyl)oleamide was constructed and validated for the fast screening of juice samples for ethyl propionate. The wide linear concentration range (between 1×10^{-15} and 1×10^{-4} mol L^{-1}) facilitates determination of ethyl propionate from ultra trace amounts to high amounts of ethyl propionate. The limit of quantification was 1 fmol L^{-1}. The high average recovery of ethyl propionate in juice samples 99.87 % with low relative standard deviation (0.10 %) proved the reliability of the proposed sensor and screening method. The 3D combined stochastic sensor can be used for the determination of ethyl propionate for at least 30 days. The feature is utilization of this screening method for on-site quality control of the juice in supermarket.

Comparative analysis of chromatographic methods vs. sensor-based detection methods.

Criteria	**Chromatographic methods**	**Sensor-Based Methods**
Time of analysis	Hours–days	Minutes
Cost per analysis	High	Low–moderate
Equipment requirements	Specialized laboratories	Portable instruments
Sensitivity and selectivity	Very high	High (improving)
Field applicability	Limited	Excellent

This table is showing the advantages of the proposed tools/methods for the determination of food additives, and nutrients in food. There is clear evidence that the proposed tools and methods are excellent alternative for chromatographic methods – used for food control in accredited laboratories. They can be used for on-site analysis of food and they will be able to highly contribute to food security.

Original contributions

New electrochemical sensors were proposed as tools for screening of bread and mayonnaise for sorbic acid. Two sensors based on nanographene decorated with gold nanoparticles paste modified with metal porphyrins (Zn protoporphyrin IX, and 2,3,7,8,12,13,17,18 octaethyl, 21H, 23H-porphirine Mn(III) chloride) were designed, characterized and validated for the determination of sorbic acid in food (bread and mayonnaise) using square wave voltammetry.

Two stochastic sensors were developed, characterized, and validated for the determination of S- and R-limonene in beverages using stochastic sensors based on immobilization of 5,10,15,20-tetraphenyl-21H,23H-porphine (TPP) and of 5,10,15,20-tetrakis(pentafluorophenyl)-21H,23H-porphyrin iron (III) chloride [Fe(TPFPP)]Cl in reduced graphene oxide decorated with Pd(0) and with gold nanoparticles.

Two voltammetric sensors based on sulfur-doped graphene (S-Gr), gold nanoparticles paste modified with 5,10,15,20-tetraphenyl-21H,23H-porphine (TPP) and 5,10,15,20-tetrakis(pentafluorophenyl)-21H,23H-porphyrin iron(III) chloride [Fe(TPFPP)Cl] were designed, characterized, and validated for determination of R-limonene in beverages. Selection of an iron complex of porphyrin versus a porphyrin was to check the effect of iron complex on the electrocatalytic oxidation of limonene versus the electrocatalytic oxidation effect of TPP on limonene.

A voltametric sensor based on 5,10,15,20-tetraphenyl-21H,23H-porphine (TPP) physically immobilized in a paste formed by mixing graphene nanopowder and paraffin oil was design, characterized, and used for on-site monitoring of atrazine in food and water.

A new platform based on stochastic sensors was designed as new tools for on-site fast screening of water and food for atrazine. The platform was able to be used on-site in different places where the monitoring of water is essential for the state of health of people, and in the supermarkets to check the quality of fruits and vegetables. The results will be able to be sent via wireless to a smart phone, computer, or data base of a specialized entity, responsible for the quality of water, or quality of food. The results of the analysis are available in maximum 6 minutes. The design of the sensors is based on physical immobilisation of 4-tert-butylcalix[4] arene, calix[4]arene-25,26,27,28-tetrol on graphite paste (graphite powder and paraffin oil). The construction of the platform was done in our laboratory using a 3D printer. While the role of calix[4]arenes is to provide the necessary channels for stochastic sensing, the graphite is assuring the conductivity of the stochastic sensor.

A 3D stochastic sensor designed using a 3D printer in the way that the reference (Ag/AgCl) and the auxiliary (Pt) sensors are set in the same 3D shape like the working – stochastic sensor which was based on physically immobilisation of calix[4]arene in nanocarbon paste was proposed for the determination of ß-carotene. Also, the 3D sensor is connected to a portable minipotentiostate which can perform data acquisition and procession and it is also able to send the data to a specialised platform for food security.

Two stochastic sensors based on nanographene powder, decorated with copper oxide nanoparticles and spheroidal copper particles and modified with β cyclodextrins, were designed, and incorporated in miniplatforms. The miniplatforms were used for enantioanalysis of L- and D- aspartic acid in biological samples, such as whole blood, saliva, and tumoral tissue, as well as in the food samples, such as hot dog, milk, egg yolk, simple yoghurt and yoghurt whey. The novelty of the screening method is that the two enantiomers of aspartic acid can be simultaneously assayed using the stochastic sensors without processing in any way both types (food/biological) of samples.

A novel 3D combined stochastic sensor based on reduced nanographene oxide paste modified with N-(pyridine-3-yimethyl)oleamide was designed and used for the fast determination of ethyl propionate in juices. N-(pyridine-3-yimethyl)oleamide is the molecule providing the necessary channel for the stochastic signal expression, because its V-shape. Reduced nanographene oxide – a material used often in sensors' technology, was selected due to its capacity of keeping the V-shape type of channel stable; this property is essential for the reliability of the response of the stochastic sensor.

Future perspectives

The new devices proved to reliable determine the substances of interest from food samples. They are able to make a huge difference in food security in any country. A reliable wireless connection had to be established between the device and a platform of authorities. Validation of all of these devices in the supermarkets with wireless submission of data to the authorities will make possible their utilisation for food security.

Because the proposed sensors can be used for more than one analyte determination, there is a possibility to increase the number of substances analysed, and in this way to have a full map of hazardous substances as well as of nutrients from food. This type of analysis made on-site in supermarkets will increase the food security and will also contribute to the state of health of population.

References

1. Ni, Z.; Zhao, J.; Nie, Y.; Gai, Z.; Tian, Z.; Li, Y.; Xin, J. Recent advances of techniques for mycotoxins analysis based on nanomaterials in food and herbal medicine: From design to applications, Food Contr., 2026, 180, 111597
2. Hu, G.; Li, X.; Zhou, B.-B.; Ma, Q.; Meng, X.; Liu, Y.; Chen, Y.; Liu, X. How to minimize the impacts of urban expansion on farmland loss: Developing a few large or many small cities? Landsc. Ecol. 2020, 35, 2487–2499.
3. Bren d'Amour, C.; Reitsma, F.; Baiocchi, G.; Barthel, S.; Güneralp, B.; Erb, K.-H.; Haberl, H.; Creutzig, F.; Seto, K.C. Future urban land expansion and implications for global croplands. Proc. Natl. Acad. Sci. USA 2017, 114, 8939–8944.
4. Cao, C.; Wang, J. The impact of urban expansion on food production: A bibliometric study of development, hotspots, and future prospects. Front. Sustain. Food Syst. 2025, 9, 1550373.
5. Seto, K.C.; Ramankutty, N. Hidden linkages between urbanization and food systems. Science 2016, 352, 943–945.
6. Zhang, Y.; Wang, H.; Xie, P.; Rao, Y.; He, Q.; Swapan, M. Revisiting Spatiotemporal Changes in Global Urban Expansion during 1995 to 2015. Complexity 2020, 2020, 11.
7. Martellozzo, F.; Ramankutty, N.; Hall, R.J.; Price, D.T.; Purdy, B.; Friedl, M.A. Urbanization and the loss of prime farmland: A case study in the Calgary–Edmonton corridor of Alberta. Reg. Environ. Change 2015, 15, 881–893.
8. Tian, G.; Ma, B.; Xu, X.; Liu, X.; Xu, L.; Liu, X.; Xiao, L.; Kong, L. Simulation of urban expansion and encroachment using cellular automata and multi-agent system model—A case study of Tianjin metropolitan region, China. Ecol. Indic. 2016, 70, 439–450.
9. Wang,S.; Bai, X.; Zhang, X.; Reis, S.; Chen, D.; Xu, J.; Gu, B. Urbanization can benefit agricultural production with large-scale farming in China. Nat. Food 2021, 2, 183–191.
10. Zhou,X.; Li, X.; Song, W.; Kong, X.; Lu, X. Farmland transitions in China: An advocacy coalition approach. Land 2021, 10, 122.
11. Yang, Y.; Zhang, D.; Nan, Y.; Liu, Z.; Zheng, W. Modeling urban expansion in the transnational area of Changbai Mountain: A scenario analysis based on the zoned Land Use Scenario Dynamics-urban model. Sustain. Cities Soc. 2019, 50, 101622.
12. Li, J.; Song, W. Food security review based on Bibliometrics from 1991 to 2021. Foods 2022, 11, 3915.

13. Huang, Q.; Liu, Z.; He, C.; Gou, S.; Bai, Y.; Wang, Y.; Shen, M. The occupation of cropland by global urban expansion from 1992 to 2016 and its implications. Environ. Res. Lett. 2020, 15, 084037.
14. Song, W.; Liu, M. Farmland conversion decreases regional and national land quality in China. Land Degrad. Dev. 2017, 28, 459–471.
15. Song, W.; Yang, D.; Wang, Y. Integrating an abandoned farmland simulation model (AFSM) using system dynamics and CLUE-S for sustainable agriculture. Agric. Syst. 2024, 219, 104063.
16. Li, L.; Wang, L.; Qi, Z. The spatiotemporal variation of farmland use transition and its critical influential factors in coordinated urban-rural regions: A case of Chongqing in western China. Sustain. Cities Soc. 2021, 70, 102921.
17. Liu, Y.; Song, W. Modelling crop yield, water consumption, and water use efficiency for sustainable agroecosystem management. J. Clean. Prod. 2020, 253, 119940.
18. Bonye, S.Z.; Yiridomoh, G.Y.; Derbile, E.K. Urban expansion and agricultural land use change in Ghana: Implications for peri-urban farmer household food security in Wa Municipality. Int. J. Urban Sustain. Dev. 2021, 13, 383–399.
19. Song, W.; Deng, X. Effects of Urbanization-Induced cultivated land loss on ecosystem services in the North China Plain. Energies 2015, 8, 5678–5693.
20. Sarangi, M.K.; Selvaraj, M.; Karnwal, A. Antimicrobial efficacy of metal-organic framework-modulated nanocomposites in foods and their contact surfaces against Staphylococcus aureus. Food Control, 2026, 179, 111574.
21. Barthel, S.; Isendahl, C.; Vis, B.N.; Drescher, A.; Evans, D.L.; van Timmeren, A. Global urbanization and food production in direct competition for land: Leverage places to mitigate impacts on SDG2 and on the Earth System. Anthr. Rev. 2019, 6, 71–97.
22. Song, W.; Song, W. Cropland fallow reduces agricultural water consumption by 303 million tons annually in Gansu Province, China. Sci. Total Environ. 2023, 879, 163013.
23. Wang,H.; Mei, Y.; Ren, J.; Zhu, X.; Qian, Z. Multi-Scale temporal integration for enhanced greenhouse gas forecasting: Advancing climate sustainability. Sustainability 2025, 17, 3436.
24. Li, W.; Diehl, J.A.; Chen, M.; Herr, C.M.; Stouffs, R. The combined effects of multiple factors on farmland and built-up land landscape patterns-A case study of Chengdu, China. Ecol. Indic. 2024, 167, 112572.

25. Yan, Z.; Li, W.; Wang, D. Outward expansion or networked growth? Comparing farmland loss in evolving urban agglomerations across Mollisol regions in the northern hemisphere. Cities 2023, 133, 104106.
26. Rulli, M.C.; Saviori, A.; D'Odorico, P. Global land and water grabbing. Proc. Natl. Acad. Sci. USA 2013, 110, 892–897.
27. Li, H.; Song, W. Spatial transformation of changes in global cultivated land. Sci. Total Environ. 2023, 859, 160194.
28. Liu, Y.; Song, W. Mapping human appropriation of net primary production in agroecosystems in the Heihe River Basin, China. Agric. Ecosyst. Environ. 2022, 335, 107996.
29. Liu, Z.; Wang, J.; Wang, X.; Wang, Y. Understanding the impacts of 'Grain for Green' land management practice on land greening dynamics over the Loess Plateau of China. Land Use Policy 2020, 99, 105084.
30. Song, W.; Deng, X.; Liu, B.; Li, Z.; Jin, G. Impacts of Grain-for-Green and Grain-for-Blue policies on valued ecosystem services in Shandong Province, China. Adv. Meteorol. 2015, 2015, 213534.
31. Li, F.; Wu, S.; Liu, H.; Yan, D. Biodiversity loss through cropland displacement for urban expansion in China. Sci. Total Environ. 2024, 907, 167988.
32. Jiang, C.; Song, W. Degree of abandoned cropland and socioeconomic impact factors in China: Multi-Level analysis model based on the farmer and district/county levels. Land 2022, 11, 8.
33. Haile Aboye, B.; Gebre-Egziabher, T.; Kebede, B. Peri-urban food insecurity and coping strategies among farm households in the face of rapid urbanization in Sub-Saharan Africa: Evidence from Ethiopia. Res. Glob. 2024, 8, 100200.
34. Salem, M.; Tsurusaki, N. Impacts of rapid urban expansion on Peri-Urban landscapes in the global south: Insights from landscape metrics in Greater Cairo. Sustainability 2024, 16, 2316.
35. Crush, J.; and Frayne, B. Supermarket expansion and the informal food economy in Southern African cities: Implications for urban food security. J. S. Afr. Stud. 2011, 37, 781–807.
36. Olivia, S.; Boe-Gibson, G.; Stitchbury, G.; Brabyn, L.; Gibson, J. Urban land expansion in Indonesia 1992-2012: Evidence from satellite-detected luminosity. Aust. J. Agric. Resour. Econ. 2018, 62, 438–456.

37. Liu, Y.; Song, W.; Deng, X. Changes in crop type distribution in Zhangye City of the Heihe River Basin, China. Appl. Geogr. 2016, 76, 22–36.
38. Sadian, A.; Shafizadeh-Moghadam, H. The future of agricultural lands under the combined influence of shared socioeconomic pathways and urban expansion by 2050. Agric. Syst. 2025, 224, 104234.
39. Wang,J.; Zhang, Z.; Liu, Y. Spatial shifts in grain production increases in China and implications for food security. Land Use Policy 2018, 74, 204–213.
40. Liu, Y.; Ou, C.; Liu, Y.; Cao, Z.; Robinson, G.M.; Li, X. Unequal impacts of global urban–rural settlement construction on cropland and production over the past three decades. Sci. Bull. 2025, 70, 1699–1709.
41. Hernandez-Vasquez, A.; Visconti-Lopez, F.J.; Chacon-Torrico, H.; Azanedo, D. COVID-19 and food insecurity in Latin America and the Caribbean. J. Hunger Environ. Nutr. 2023, 18, 372–379.
42. Shita, M.W.; Agegnehu, S.K.; Nurie, D.F.; Dires, T.; Navratil, G. Factors affecting food security of expropriated Peri-Urban households in Ethiopia: The case of the East Gojjam Administrative Zone. Land 2024, 13, 1779.
43. Milan, T.; Martens, C. Venezuelan Migration, COVID-19 and Food (in)Security in Urban Areas of Ecuador. Land 2023, 12, 517.
44. Sangroniz, A.; Ebel, R.; Stein, M. Barriers and opportunities to agrihood development in growing cities of the Rocky Mountain Region: A comparative case study. J. Agric. Food Syst. Community Dev. 2024, 13, 271–288.
45. Kovljenic, M.; Matkovski, B. Food security challenges: Evidence from the southeast Europe countries. Biotechnol. Agron. Soc. Environ. 2024, 28, 91–101.
46. Shen, X.; Zhang, D.; Nan, Y.; Quan, Y.; Yang, F.; Yao, Y. Impact of urban expansion on grain production in the Japan Sea Rim region. Front. Earth Sci. 2023, 10, 1025069.
47. Borras, S.M., Jr.; Franco, J.C.; Gomez, S.; Kay, C.; Spoor, M. Land grabbing in Latin America and the Caribbean. J. Peasant Stud. 2012, 39, 845–872.
48. Song, W.; Han, Z.; Deng, X. Changes in productivity, efficiency and technology of China's crop production under rural restructur ing. J. Rural Stud. 2016, 47, 563–576.
49. Olsson, E.G.A.; Kerselaers, E.; Søderkvist Kristensen, L.; Primdahl, J.; Rogge, E.; Wästfelt, A. Peri-Urban food production and Its relation to urban resilience. Sustainability 2016, 8, 1340.
50. Xiong, R.; Peng, H.; Chen, X.; Shuai, C. Machine learning-enhanced evaluation of food security across 169 economies. Environ. Dev. Sustain. 2024, 26, 26971–27000.

Annex1 Participation in national and international conferences

1. **Andreea-Roxana Niculae**, Raluca-Ioana Stefan-van Staden, Jacobus (Koos) Frederick van Staden, Ultrasensitive assay of atrazine in food and water samples - **poster**, Transnational Multiplier event of REALME project - A Mixed Reality E-Learning Platform Dedicated for Medical Engineering, 18 – 19 OCTOBER 2023, National University of Science and Technology POLITEHNICA Bucharest.

2. **Andreea-Roxana Niculae**, Raluca-Ioana Stefan-van Staden, Fast screening of biological and food samples using miniplatforms based on 3D stochastic microsensors - **poster**, Transnational Multiplier event of REALME project - A Mixed Reality E-Learning Platform Dedicated for Medical Engineering, 18 – 19 OCTOBER 2023, National University of Science and Technology POLITEHNICA Bucharest.

3. Raluca-Ioana Stefan-van Staden, **Andreea Roxana Niculae,** Rasit Ergün Yukmel, Damaris-Cristina Gheorghe, Jacobus (Koos) Frederick van Staden, Sensitive platforms for fast on-site screening of food – **oral presentation**, Euroanalysis XXI, Geneva, Switzerland, 27-31 August, 2023.

3. **Andreea-Roxana Niculae**, Raluca-Ioana Stefan-van Staden, Jacobus (Koos) Frederick van Staden, Ultrasensitive assay of atrazine in food and water samples - **poster**, Euroanalysis XXI, Geneva, Switzerland, 27-31 August, 2023.

4. **Andreea-Roxana Niculae**, Raluca-Ioana Stefan-van Staden, Fast screening of biological and food samples using miniplatforms based on 3D stochastic microsensors - **poster**, Euroanalysis XXI, Geneva, Switzerland, 27-31 August, 2023.

5. **Andreea Roxana Niculae**, Raluca-Ioana Stefan-van Staden, Jacobus Frederick van Staden, Ruxandra-Maria Ilie-Mihai, Fast screening of biological and food samples using miniplatforms based on 3D stochastic microsensors – **poster**, Eurachem Workshop Complex Matrices:

Applications, Laboratory Standards, and Accreditation, Bucharest, ROMANIA - May 26 – 27, 2025.

6. **Andreea Roxana Niculae**, Raluca-Ioana Stefan-van Staden, Jacobus (Koos) Frederick van Staden, Ultrasensitive and fast determination of ß-carotene in vegetables using stochastic sensors - **poster**, Eurachem Workshop Complex Matrices: Applications, Laboratory Standards, and Accreditation, Bucharest, ROMANIA - May 26 – 27, 2025.

Annex 2 Paper published in ISI Journals

Sulfur-doped graphene based electrochemical sensors for fast and sensitive determination of (R)-(+)-Limonene from beverages
AR Niculae, RI Stefan-van Staden, JF van Staden, R Georgescu State
Sensors, 22(15), 5851 https://doi.org/10.3390/s22155851, 2022 **Q2**

Electroanalysis of atrazine in water and beverages
AR Niculae, RI Stefan-van Staden
UPB Sci Bull, 86(1), 72-80, 2024

Ultrasensitive and fast determination of ß-carotene in vegetables using stochastic sensors
AR Niculae, RI Stefan-van Staden, JF van Staden
Anal.Lett., 58, 2820-2827, 2025 **Q3**

Fast screening of biological and food samples using miniplatforms based on 3D stochastic microsensors
AR Niculae, RI Stefan-van Staden, JF van Staden, RM Ilie-Mihai
Journal of the Electrochemical Society, 172, 077507, 2025 **Q2**

Nanographene based electrochemical sensors for ultrasensitive determination of sorbic acid from bread and mayonnaise
RI Stefan-van Staden, **AR Niculae**, JF van Staden, P Sfirloaga, R State
Anal Bioanal Chem, 414(23), 6813–6824, 2022 **Q1**

Ultrasensitive assay of atrazine in food and water samples
RI Stefan-van Staden, **RA Niculae**, JF van Staden
Electroanalysis, 35(12), e202300248, 2023 **Q3**

Stochastic enantioselective microsensors used for enantioanalysis of limonene in beverages
RI Stefan-van Staden, **AR Niculae**, JF van Staden
Journal of the Electrochemical Society, 171(9), 097514, 2024 **Q1**